Catalysis Science & Technology

rsc.li/catalysis

Volume 7
Number 2
21 January 2017
Pages 313–534

ISSN 2044-4761

ROYAL SOCIETY OF CHEMISTRY

PAPER
Chaoqiu Chen, Yong Qin *et al.*
Highly dispersed Pt nanoparticles supported on carbon nanotubes produced by atomic layer deposition for hydrogen generation from hydrolysis of ammonia borane

ROYAL SOCIETY OF CHEMISTRY

rsc.li/catalysis

Recent Advancements of Pt-nanostructure Based Electrocatalysts for Oxygen Reduction Reaction

Arup Mahata,[†] Akhil S. Nair,[†] Biswarup Pathak,[†,#,*]

[†]Discipline of Chemistry and [#]Discipline of Metallurgy Engineering and Materials Science, Indian Institute of Technology (IIT) Indore, Indore. M.P. 453552, India

Email: biswarup@iiti.ac.in

Abstract

Developing highly efficient and durable electrocatalysts for oxygen reduction reaction (ORR) is the key to the performance of proton exchange membrane fuel cells (PEMFC) for future energy applications. Pt-based electro catalysts show the greatest promise for this reaction among which nanostructure-based catalysts have been identified as potential candidates owing to their morphological, geometrical, size dependent activities revealed from experimental and theoretical studies. The fundamental aspects of origin of activity enhancement of nanostructure-based catalysts are manifested in the finest form in recent advancements in ORR catalyst designing process. Also, it is one of the areas of research where theoretical studies have contributed to a significant extent in developing tools and techniques which are currently applied in a wide regime in the electrocatalysis scenario beyond the fuel cell catalysis. This review covers the recent progress in the Pt-based nanostructure catalysts for ORR. The review delves into a comprehensive analysis of effective utilization of theoretically obtained insights in the experimental designing of efficient Pt-nanostructure ORR catalysts as well as identifying the origin of their activities. A detailed discussion of ORR mechanism on low and high-index facets, nanostructure morphologies, composition, shape and size dependent activities of Pt-based

catalysts is included emphasizing from theoretical perspectives. The underlying factors behind the experimentally reported excellent ORR activities of nanostructure based catalysts are analysed from a detailed investigation of theoretically important factors such as binding energy, reaction barrier, overpotential and strain effects. Finally, challenges and future research directions towards experimental designing of efficient ORR catalysts by using the knowledge gained from theory are also addressed.

1. Introduction

The oxygen reduction reaction (ORR) has long been a topic of extensive research in developing proton exchange membrane (PEM) fuel cells as the slow reaction kinetics associated with ORR and high Platinum (Pt) loading in a state-of-the-art ORR electrocatalyst (Pt/C) remains as a hurdle for the commercialization of PEM fuel cells.[1-5] However, platinum is the best electrocatalyst for ORR with high activity and durability in acidic as well as alkaline media.[6,7] On the other hand, the reaction rate of hydrogen evolution reaction (HER) at the Pt-anode is around 5 times higher than ORR and hence the Pt-loading required at the anode is very less.[8] Therefore, it is the cathode of a PEM fuel cell which typically contains 80–90% of the total Pt of the cell.[9] Due to the low abundancy of Pt, Unite States Department of Energy has set the target of total Pt-loading (anode + cathode) below 0.125 mg/cm^2 in 2017, while the present status of loading on cathode is 0.4 mg/cm^2 or more.[10] Although many efforts towards Pt-free electro-catalysts such as non-precious transition metals,[11-13] metal nitrides,[14-16] chalcogenides[17,18] and nanoscale carbon-based metal-free electrocatalysts[19-21] have been devoted, the poor stability, limited performance and the higher cost of implementation as compared to Pt electrocatalysts prevent their commercialization for the fuel cell industry.[22,23] Therefore, the development of a

catalyst with less Pt-loading without compromising the performance of the ORR is a need of the hour and probably the solemn solution for lowering the fuel cell cost. This can be achieved either by reducing the amount of Pt or by changing the morphology of the Pt catalyst. In this regard, different category of catalysts like core–shell nanoparticles,[24-26] hollow nanomaterials,[27-29] ultrathin nanosheet catalysts[30,31] and so on have been proposed and found to be efficient for ORR activity. Furthermore, the catalytic activity of the Pt-based catalysts can be improved by tuning the morphology, i.e. designing nanoparticles selectively enclosed by high and low index facets.

In recent years, a substantial amount of research efforts based on computational and experimental studies have been devoted towards the design and synthesis of electrocatalysts with high activity and durability for ORR, the results and conclusions of which have undergone comprehensive review before.[32,33,35-39] Shao et al.[32] comprehensively reviewed the recent development of ORR electrocatalysts with novel structures and compositions focusing on the low and non-platinum electrocatalysts including advanced platinum alloys, core−shell structures, palladium-based catalysts, metal oxides, chalcogenides, carbon-based non-noble metal catalysts and metal-free catalysts in acidic media. The review by Nie et al.[33] covers the catalyst material selection, design, synthesis and characterization. Further, they have shed a light on the theoretical understanding of the ORR mechanisms proposed by Nørskov et al.[34] Research groups led by Goddard,[35] Anderson[36] and Jiao[37] have nicely reviewed the key parameters of clean energy conversion reactions including ORR, oxygen evolution reaction (OER), and HER via both theoretical and experimental considerations. Keith and coworkers reviewed the investigations of ORR on Pt (111), focusing on the theoretical aspects of different types of quantum mechanical simulations approaches to create a realistic model of ORR.[38] In a very

recent review by Nørskov et al.,[39] they have scrutinized the descriptor-based approaches in ORR and summarized the alternative strategies for enhancing the catalytic activity.

Nevertheless of some nice reviews focused on the ORR mechanism and progress on the performance of nanostructured catalysts, the fundamental theoretical insights behind the excellent catalytic activity and stability of the breakthrough nanostructures architect towards ORR have not been exclusively reviewed so far. In spite of enormous experimental reports driven as well as supported by theoretical studies for the excellent activity of Pt-nanostructure catalysts, the essential factors enabling the correlation between theoretical and experimental strategies have not been subjected to an extensive discussion. More importantly, how the adsorption behaviour of the intermediates, rate determining steps and reaction pathways of ORR are controlled by the various nanostructured catalysts have not been addressed. In addition to that, the underlying reason, alongside the so called strain and ligand effect rendering the exceptional behavior of the nanostructure catalysts has not been comprehensively summarized. What is more, the role of morphology and size of the nanoparticle catalysts towards ORR activity has not been reviewed so far from theoretical aspects. Therefore, in this review, we provide an overview of the recent advancements towards understanding as well as developing efficient Pt-based catalysts for ORR grounded on theoretical studies. By attempting to explain how the efforts for achieving superior ORR activity have been supported by theoretical insights, we try to conjoin the models and techniques used in theoretical studies to the experimental framework. The review begins with a discussion on the current understanding of the ORR mechanism and its dependency on various reaction parameters such as coverage, solvent effect, adsorption energetics and so on from a theoretical perspective. It is followed by a discussion on the recent advancements in ORR activity of the less explored high-index surfaces. Then, the
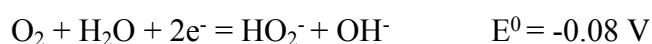
breakthrough findings of Pt-based catalysts with various geometric architectures and catalyst compositions (e.g nanocage, sheets, core-shell, alloy etc.) are summarized and the underlying reasons behind their excellent activity and stability are discussed. Meanwhile, significant attention is given on the activity of alloy based catalysts. The successful utilization of theoretically derived models and principles for understanding the stability, selectivity and activities of various nanostructure morphologies is examined. Further, the review illustrates the effect of shape and size of catalysts on ORR performance. The review is concluded by summarizing the major challenges and research directions in order to shed light on the future development of ORR catalysts.

2. Mechanism of ORR

During the ORR, H_2O and H_2O_2 are the two end products, which are formed via four-electron ($4e^-$) and two-electron ($2e^-$) reduction reactions, respectively.[40,41] The overall reactions for the reduction process in acidic medium are as follows:

$O_2 + 4H^+ + 4e^- = 2H_2O$ $E^0 = 1.23$ V

$O_2 + 2H^+ + 2e^- = H_2O_2$ $E^0 = 0.69$ V

$H_2O_2 + 2H^+ + 2e^- = 2H_2O$ $E^0 = 1.76$ V

On the other hand, the overall reactions in alkaline medium are as follows:

$O_2 + 2H_2O + 4e^- = 4OH^-$ $E^0 = 0.40$ V

$O_2 + H_2O + 2e^- = HO_2^- + OH^-$ $E^0 = -0.08$ V

$HO_2^- + H_2O + 2e^- = 3OH^-$ $E^0 = 0.88$ V

At the potential between 0.8 and 0.9 V, under which PEMFCs typically operate, oxygen gas adsorbs on the surface layer of catalysts, followed by reduction to form water via the combination of many electrochemical and thermochemical pathways. Pt-based catalysts are

mainly used under acidic conditions whereas the non-noble metals and their oxides are stable in alkaline medium.[42,43] The two-electron reduction of H_2O_2 to H_2O is not favourable in the reaction, therefore this process is generally not considered in the studies. In our previous studies, we have studied two pathways (direct and indirect) for the reduction process as shown in Fig. 1A.[44,45] For the 4e⁻ reduction (H_2O formation), the reaction can proceed through both direct and indirect pathways. In the direct pathway, the adsorbed oxygen molecule (*O_2) undergoes direct O–O bond dissociation (*O_2 → *O + *O) and in the indirect mechanism, the reaction proceeds via hydrogenation of adsorbed O_2 species (*O_2 + *H → *OOH) followed by dissociation. In the direct pathway, atomic *O may undergo two subsequent protonations to form water. On the other hand, the indirect mechanism can follow two pathways i.e. through peroxyl and peroxide formations. In the peroxyl mechanism, *O_2 undergoes hydrogenation (*O_2 + *H → *OOH) followed by dissociation (*OOH → *O + *OH). Then the product (*OH) further undergoes subsequent hydrogenation for the formation of H_2O (major product). In the peroxide mechanism, *OOH can undergo further hydrogenation leading to the formation of *H_2O_2 which involves a two-electron reduction. However, *H_2O_2 can again dissociate into *OH, which can undergo further protonation for the formation of H_2O. Based on these reaction intermediates and elementary steps, a significant extent of theoretical and experimental understanding has been obtained for different electrocatalysts and reaction conditions.[46-48]At low potentials and low coverage, ORR follows the dissociation pathway via first order reaction kinetics, where the O-O bond breaks before its hydrogenation. In contrast, at high potentials and high coverage, ORR follows a higher order kinetics and *OOH has been considered as first intermediate during the reaction course.[49-52] Stamenkovic et al.[53] demonstrated a relationship between binding energy of intermediates and reaction mechanism on Pt-based catalysts. They reported that the ORR activity

is limited by the rate of removing surface oxides and anions from surface when the catalyst binds oxygen too strongly on the surface. On the other hand, when the catalyst binds oxygen too weakly, the transfer of electron and proton to adsorbed O_2 becomes the rate determining step.
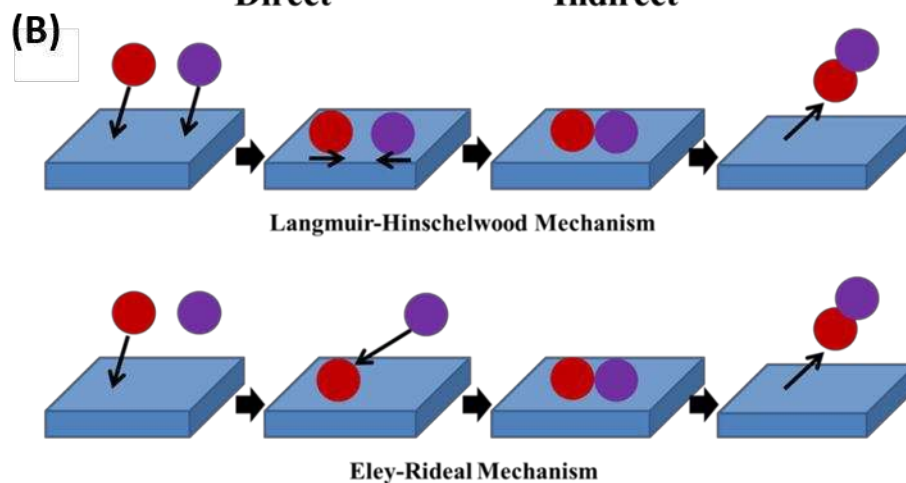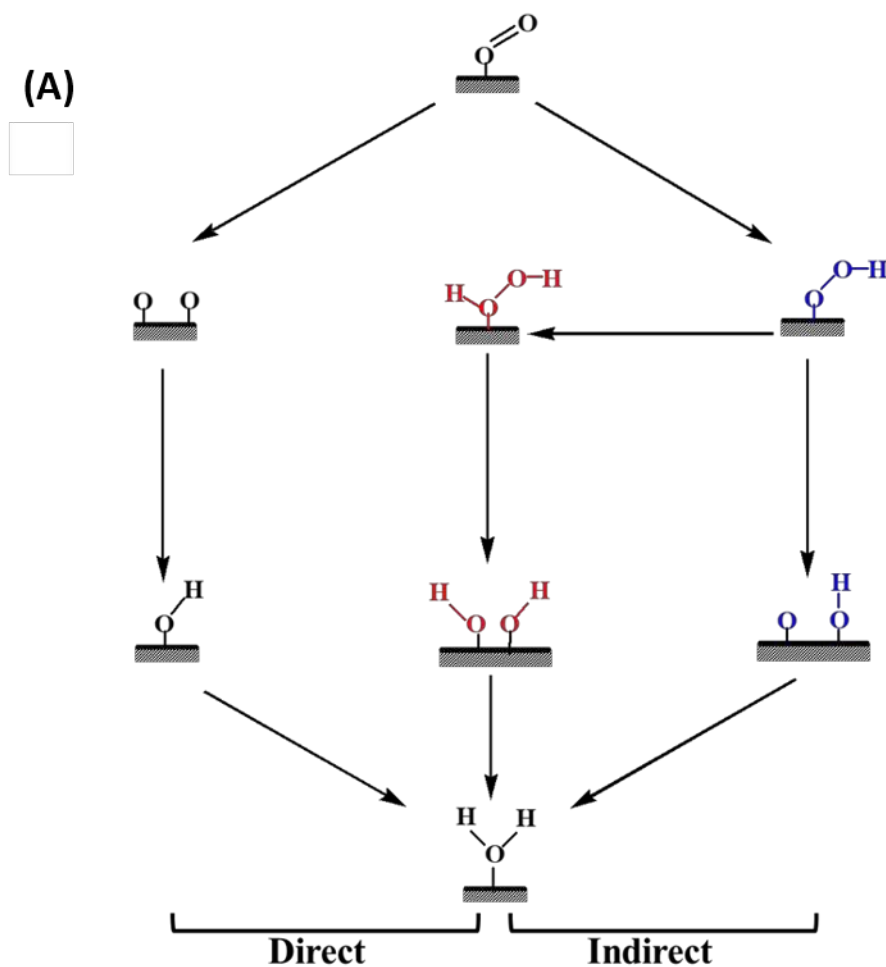
Fig. 1: (A) Possible reaction intermediates and elementary steps for oxygen reduction and (B) schematic representation of Langmuir-Hinschelwood and Eley-Rideal mechanism.

Investigations on rate determining steps and sequence of electron and proton transfer during ORR have been done in the recent past, majority of them based on density functional theory (DFT) which works well for solids and surfaces. Results from the respective studies have contributed significantly in gaining an atomic scale understanding of the mechanism of ORR and hence subsidized the experimental efforts for optimizing parameters of improved catalytic activity.[54] Using GGA-PBE level of theory and (2×2) supercell of Pt (111) surface, Ou and Chen[55] observed hydrogenation of *O towards *OH formation as a rate determining step. Using similar level of theory, Li et al.[56] also reported *OH formation as the rate determining step on (3×3) supercell of Pt (111) surface. These studies include a thermodynamic as well as kinetic analysis of elementary ORR steps with free energy and activation energy barrier calculations, respectively. Duan and coworkers also identified *O protonation step as rate limiting for ORR on a (2×2) Pt (111) supercell using GGA-PW91 calculation.[57] By fitting the reaction enthalpies and activation energies via Bell–Evans–Polany (BEP) relation and extrapolating to obtain values corresponding to zero heat of reaction, the authors observed that consideration of positive applied potential do not change the expected mechanism and rate determining step on Pt or Pt/M surfaces. Similar consistency of the rate determining step and favourable mechanistic pathways has been observed from potential dependent activation barrier analyses in the previous reports from our groups as well.[31] Similarly, a higher *OH formation barrier (0.74 eV) compared to O_2 dissociation (0.44 eV) and O_2 hydrogenation (0.30 eV) was inspected by Goddard and co-workers[58] in their gas phase study on (2 x 2) Pt (111) surface.

In this context, several theoretical reports are available on the coverage dependence of ORR on Pt (111) surface as it plays a vital role in determining the adsorption energy of intermediates. Loffreda and coworkers demonstrated that decreasing the coverage from 1/4 to 1/12 ML (monolayer) stabilizes the oxyl species like *O, *OH and *OOH, whereas the stabilization effect is very less for molecular adsorbates such as O_2, H_2O and H_2O_2.[59] Due to the strong adsorption behaviour of O-atom, the $*O_2$-dissociation reaction becomes highly exothermic at low coverage and water is likely formed by the direct oxygen dissociation route, and not via the OOH intermediates. Qi and collegues[60] have also offered similar arguments that O_2-dissociation barrier becomes lower at low coverage and they reproduced the barrier of 0.3 eV which is very much close to the experimental O_2-dissociation barrier.[61] Differently, Janik and co-workers[62-64] ascertained that the first electron transfer precedes via the protonation of the adsorbed O_2 molecule, where the proton remains as a H_3O^+ species, which interacts to the adsorbed O_2 molecule via hydrogen bonding with two additional water molecules. Similarly, Goddard and co-workers[35] proposed a mechanism, where they have demonstrated that formation of *OH possess significantly lower barrier when the process undergoes via hydration of O-atom (*O + H_2O → 2*OH) compared to hydrogenation of O-atom (*O + *H → *OH).

The inclusion of water molecules in the theoretical models can greatly influence the substrate-adsorbate interaction, which eventually alters the ORR energetics. Generally, there are three kind of computational methods are available for modelling the solvation; i) implicit model where the catalyst is engulfed in a dielectric solvent medium [65,66] ii) explicit model where individual intermediate-solvent interactions such as hydrogen bonds are considered[67,68] and iii) combined implicit-explicit where explicit solvent molecules are considered in the first solvation shell and an implicit medium beyond the first solvation shell.[69,70] Very recently, Calle-Vallejo et al.[71]

reported an inexpensive yet accurate explicit model where they showed that without any need for explicit or implicit media, a micro-solvation approach with just three water molecules captures the contribution of co-adsorbed water to the adsorption energies of *OH and *OOH on platinum nanoparticles of various sizes. Authors showed that two out of three water molecules creates H-bonds with O atoms in the adsorbates and the third water molecule creates H-bonds with their H atoms, having no effect of the up or down orientations of water molecules in the micro-solvation environments. These results lead to an accurate as well as computationally affordable channel to describe the solvent contribution in the ORR mechanism.

In this context, it is noteworthy to mention that there are two mechanisms related with the hydrogenation process. Hydrogen can react with the oxygen/oxygenated species either via Langmuir-Hinshelwood (LH) mechanism or Eley-Rideal (ER) mechanism as demonstrated in Fig.1B.[72-74] In LH mechanism, both the oxygen and hydrogen adsorb on the surface close to each other on their preferred sites and undergo a bimolecular reaction to form a product, which eventually desorbs from the surface. In case of ER mechanism, the hydrogen (from the electrolyte) reacts directly with the oxygen/oxygenated species before undergoing adsorption on the surface and the product either remains adsorbed on the surface or get desorbed depending on the elementary step. It is the LH mechanism that has been widely followed which makes energetics of *H coadsorption along with that of ORR intermediates also important in ORR studies.

Nørskov et al.[34] introduced a method for evaluating the ORR performance by calculating the free energy of all intermediates as a function of the electrode potential (Fig. 2A & B) which has been adapted in many theoretical studies. In this model, at 0V, the chemical potential of a proton-

electron pair, $\mu(H^+) + \mu(e^-)$ is equated to the half of the chemical potential of gaseous hydrogen $(1/2\mu(H_2))$ which facilitates the calculation of the chemical potential of the former. The variation of chemical potential of electron under an applied potential is included as the free energy change of $\Delta G = -eU$, where e is the elementary positive charge and U is the applied bias. Hence, variation in the applied potential varies the energetics of elementary steps of ORR and the highest potential at which all the ORR steps retain exothermicity is the theoretical onset potential of the catalyst. They constructed the free energy profile based on the adsorption energies of the surface intermediates (*O and *OH) of ORR. In this way, the ORR activity was calculated for various metals and a volcano trend appeared showing that Pt and Pd are the best catalysts for ORR (Figure 2C & D). They established that the overpotential is originating from strong binding of *O and *OH species on the surface which reduces the availability of surface sites for further steps. Similarly, the dissociation of O_2 or the transfer of electrons and proton to adsorbed O_2 for the metals which bind oxygen too weakly also limits the rate. Since all the O-mediated intermediates do exhibit a similar adsorption behaviour, the catalytic activity can be explained with respect to the adsorption energy of a single intermediate, often *O or *OH which has become the crucial activity descriptor for many studies. They established an optimal range of *O binding energy, which is ≈ 0.2 eV lower than that on the bulk Pt (111) surface for an efficient catalyst for ORR. Furthermore it is also found that for surfaces which bind oxygen intermediates too strongly, it is the reduction of *OH to H_2O is the rate determining step while for surfaces which bind oxygen intermediates too weakly, it is the protonation of adsorbed O_2 which turns to be the rate determining step.[75] However, the conclusion was drawn mainly from their reaction free energy calculations assuming that smaller the positive change in free energy, faster the corresponding reaction step. They have also developed a kinetic activity volcano which is in

close agreement with the thermodynamic activity volcano derived earlier. In this microkinetic model, an optimal *OH binding energy of 0.1 eV and 0.3 eV weaker than Pt (111) for 4e⁻ reduction and 2e⁻ reduction respectively was suggested for the maximum ORR activity which is being addressed as a more important activity descriptor than *O binding energy in the recent ORR studies.
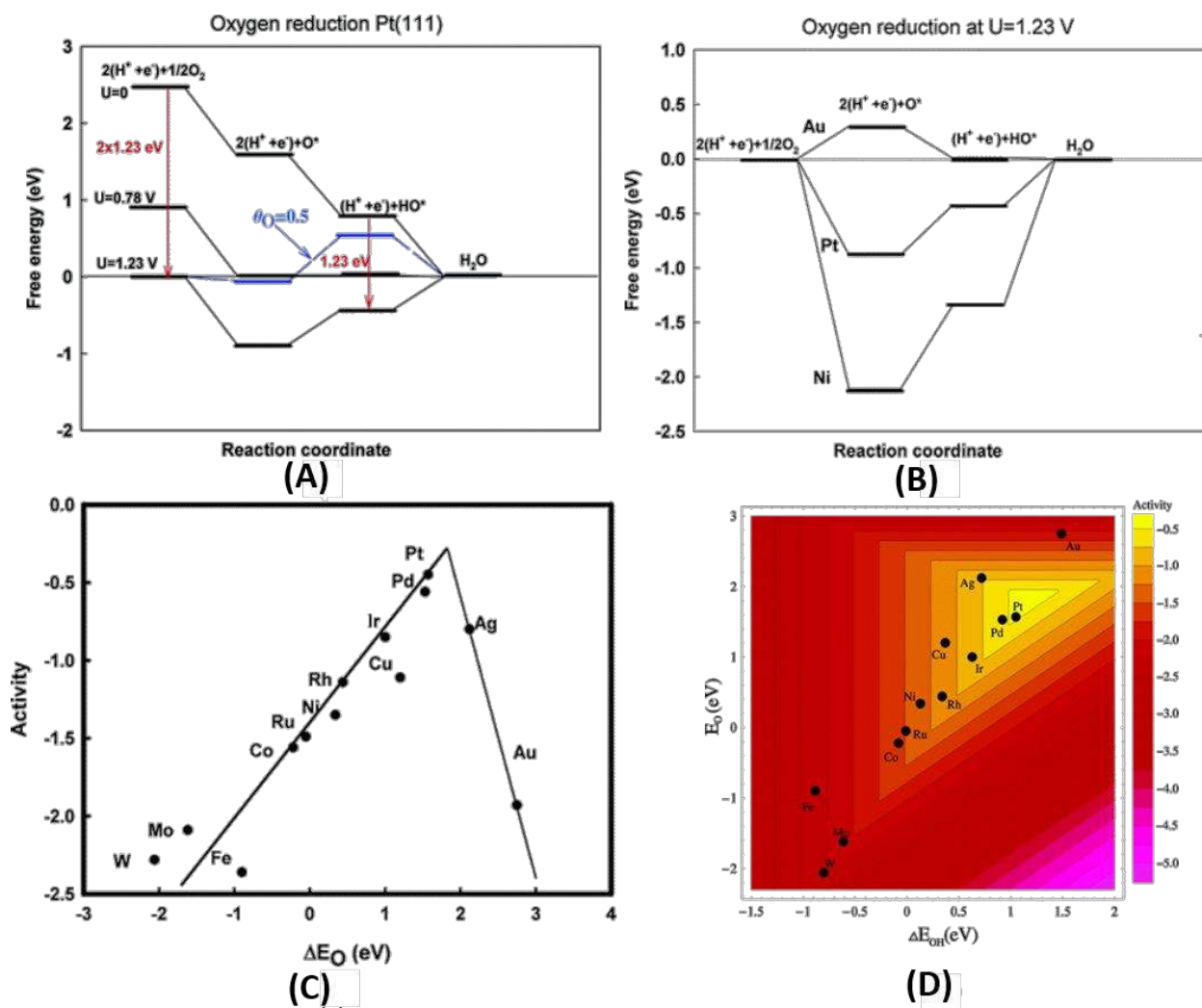

Fig. 2: Free-energy diagram for ORR on (A) Pt(111) at different applied potentials, (B) for Au, Pt, and Ni(111) at the equilibrium potential 1.23 V. ORR activity trends plotted as a function of the (C) *O binding energy and (D) both the *O and the *OH binding energy. Adapted with permission from ref. 34. Copyright 2004 American Chemical Society.

One of the important outcomes of extensive studies by Nørskov and co-workers was the exploration of scaling relationship between ORR intermediates. Though a thermodynamic study, it was Kopper,[76] who firstly reported that there exists a scaling relationship between *OH and *OOH where their adsorption strength was found to differ by a constant amount of ≈3.2 eV for transition metal (111) facets as well as oxide surfaces, irrespective of the adsorption site. The strong binding of one of the intermediates increases the rate of electron transfer step mediated by it while decreasing the rate of other step rendering the sluggish nature of ORR. Although these conclusions are made only based on reaction energies, the Brønsted–Evans–Polanyi relationship,[77,78] which imposes that the changes in the activation energy for an elementary step follow changes in the reaction energy validates these observations. A recent study by Viswanathan et al.[79] has shown that the constant scaling between *OH and *OOH and hence a universal volcano trend holds for the fcc metal (100) facets as well. Nevertheless, many recent works from different perspectives have questioned the universality of scaling relationship. Calle-Vallejo and coworkers have studied the deviation from the generally accepted scaling relation in detail. They suggested that catalyst-adsorbate interactions can be classified according to their ionic and covalent nature, where conventional scaling relations are followed when the interactions are ionic and are broken when the interactions are covalent.[80,81] In a very recent review from the group where different category of ORR/OER catalysts are studied, they have pointed out that even though breaking of this scaling is necessary for improving ORR activity, it cannot be treated as a sufficient descriptor for the design of superior catalysts.[82] Apart from the ORR intermediates, scaling relation has also been observed between recently proposed activity descriptors such as generalized coordination number,[83-85] vibrational frequencies[86] and so on.

Recently, Gagliardi and coworkers[87] have proposed a computational model based on the scaling relation between *OH adsorption energy and generalized coordination number which successfully reproduced the experimental ORR mass activities of nanoparticle catalysts. These studies reveal the possibility of emergence of more accurate and well-accepted activity descriptors for ORR.

3. Platinum catalysts and ORR activity

3.1. Low and high-index bulk Pt-surfaces

Through various experimental measurements on single crystal surfaces and computational simulations have reported, it has long been recognized that the activity and selectivity of a heterogeneous catalyst for a structure-sensitive reaction is highly dependent on the arrangement of atoms and thus the type of crystallographic plane on a surface.[88-90] This surface structure-activity relation has been utilized for the development of active Pt based electrocatalysts for decades. For platinum with a face-centered cubic (fcc) crystal structure, the (111), (100) and (110) index planes or facets are typically found on single-crystal surfaces of bulk structure. Nanocrystals with a polyhedral shape are often enclosed by (111) and (100) facets. Cubes are enclosed by (100) facets, whereas the tetrahedra, octahedra, decahedra and icosahedra are enclosed by (111) facets.[91,92] Cuboctahedral and truncated octahedral nanostructures possess a mixture of (100) and (111) facets.[93,94] Commercial Pt/C catalysts are usually bounded by low-index facets such as (100) and (111). The ORR activity of low index Pt surfaces has been extensively studied both theoretically and experimentally which have been summarized in several comprehensive reviews.[32,33] The general conclusion from the studies is that the activity of ORR in a weakly adsorbed electrolyte, such as $HClO_4$ solution, follows the order of $Pt(100) \ll Pt(111) \approx Pt(110)$ while in the strongly adsorbing electrolytes such as H_2SO_4, the ORR activity

follows the order of Pt(111) < Pt (110) < Pt(100).[95] The lesser activity on Pt (111) is due to the stronger adsorption of sulfate anion (SO_4^{2-}) on Pt (111) compared to that on Pt (100) and thus limiting the accessibility of Pt sites, which actually lowers the O_2 adsorption.[96,97] However, in this review, we discuss some recent advancements in ORR activity studies on comparatively less explored high- index surface planes.

The high-index planes have high densities of atomic steps, edges, and kinks that serve as active sites for breaking chemical bonds and thus significantly enhance catalytic activity towards specific reactions as compared to the low-index planes.[98,99] Several attempts have been taken to synthesize such high-index facet Pt nanocrystals. In a very recent review by Wilkinson's group,[100] they have comprehensively discussed the immense electrocatalytic applicability of polyhedron-engineered Pt-based nanocrystals. The authors proposed the exploration of high-index facets as an effective way to obtain highly active polyhedron-designed Pt nanocatalysts. Wang and co-workers have given a breakthrough by synthesizing thermally stable (up to 800 °C) tetrahexahedral (THH) Pt nanocrystals with high-index facets [(730), (210), and (520)] which show excellent electro-oxidation activity (formic acid and ethanol oxidation) compared to Pt (111) surface.[101] Later on, Xia and coworkers have synthesized Pt concave nanocubes enclosed by high-index facets [(510), (720), and (830)].[102] The Pt concave nanocubes exhibited substantially enhanced electrocatalytic activity per unit surface area towards ORR compared with those of Pt cubes, cuboctahedra, and commercial Pt/C catalysts that are bounded by low-index planes such as (100) and (111). However, the mass activity of Pt concave cubes is less than that of the Pt/C catalyst. The authors claimed that the smaller electrochemically active surface area per unit weight of Pt in the relatively larger particle size is responsible for lower mass activity. Lou and coworkers reported platinum nanoframes with concave (740) facets mass

activity of 13.1 A/g$_{Pt}$ at 0.80 V, which is about 1.22 and 1.68 times of that of Pt nanocubes and commercial Pt/C catalysts, respectively.[103] Although high-index surfaces might emerge as very promising catalysts for ORR, they suffer some drawbacks. The high-index nanocrystals tend to be grown in large size, which subsequently lowers the mass activity of the reaction. Furthermore, the high-index planes and unsaturated atomic steps, edges and kinks might be unstable during the reaction conditions of fuel cell. These facets may easily be deactivated due to the high dissolution rate, resulting in degradation of their catalytic activity and thus hindering their capability in practical application. Nevertheless, efficient and innovative techniques can guide to the synthesis of high-index facet nanostructures with profound stability as well as durability.

In spite of the enhanced activity, the underlying reaction mechanism on high-index surfaces is very much complicated and controversial as compared to low index surfaces. Feliu et al.[104-106] have performed extensive study on high-index surfaces in both acidic and alkaline media and reported that the ORR activity increased on the stepped surface (formed by (111) and (100)) compared to Pt (111) plane in acidic media, whereas Pt (111) surface shows highest activity compared to other basal planes and stepped surface in alkaline media. They further pointed out that orientation of step and terraces on the surface has also significant role towards catalytic activity. Hoshi's group[107] studied the structural effects on the ORR on the various types of high-index planes of Pt [n(111)–(111), n(111)–(100), n(100)–(111) and n(100)–(110)] using rotating disk electrode (RDE) in 0.1 M HClO$_4$ and agreed with the results of Feliu et al. The authors reported that surface with (111) terrace possess higher ORR activity compared to (100) terrace. They further demonstrated that the ORR activity on the surfaces with (111) terrace increases with the increase of terrace atomic rows n (except n = 2), whereas the activity does not depend on the step density on (100) terrace.

As proposed by Nørskov and coworkers, the optimal binding energy of OH species leads to the lowest overpotential and hence higher activity.[34] The common strategy employed for the utilization of this idea is alloying the Pt (111) surface with other metals leading to a weakening of *OH binding energy and hence an improvement in ORR activity.[108-110] On the other hand, low-coordinated sites such as steps bind *OH much strongly than the (111) facet,[111,112] implying that the step sites should show a high overpotential, i.e. lesser activity in comparison to Pt(111). In contrast, some Pt stepped single crystals such as [Pt [n (111) × (111)] and Pt [n (111) × (100)] show an improved ORR activity compared to Pt(111).[101,113,114] Therefore, some interesting and unique effects are expected to operate in case of high-index surface. This has been addressed by certain theoretical studies as they provide room for modelling and analyzing the activity of the under-coordinated sites on a high-index surface. A widely accepted mechanism is that ORR activity increases on several stepped Pt surfaces because the *OH adsorbates are destabilized with decreased solvation. Bandarenka et al.[115] demonstrated a volcano-plot based on the ORR activities vs. electrode potential, forming OH adsorbates in the acid electrolytes. Similar to the volcano-plot of Pt-alloy (111) surfaces, they reported that (111)-terraces are the most active sites of ORR on stepped Pt surfaces and it has been credited that OH adsorbates at the (111)-terraces get destabilized because of the decreased solvation of OH (dry OH). Later on, using DFT with Poisson–Boltzmann solvation theory, Nagoya and coworkers analyzed the formation of H, OH and O adsorbate on Pt (322) and Pt (111) and reported that the ORR activity increases on several stepped Pt surfaces because the OH adsorbates are destabilized with decreased solvation, which was supported by experimental observation of Bandarenka et al.[116] Very recently, the same group has further explained the underlying reason of the volcano-plot observed by Bandarenka et al.[117] In this study, they have analyzed the solvation behavior of the adsorbed ORR reaction

intermediates [O, OH and OOH] at the middle of the (111)-terraces on the stepped Pt surfaces [Pt(665), Pt(554), Pt(443) and Pt(332)] and reported that all the intermediates are destabilized with the decrease in the width of (111)-terrace and the destabilizations are caused mainly by the decreased solvation of the reaction intermediates. The decreases in the solvation of *O and *OOH are linearly correlated with the solvation behaviour of OH, which eventually generate the volcano-type correlation between the ORR activity vs. binding energy of OH similar with the alloy-based catalyst. Therefore, controlled solvation of reaction intermediates is a key factor for improving the ORR activity on high-index surface.

Another explanation for the higher activity of high-index facets is that the repulsive interactions from strongly adsorbed species destabilize the adsorbed *OH at neighbouring sites. Using DFT, Yue et al.[118] studied the reaction mechanism of ORR on the various sites of high-index platinum n(111)−(111) surfaces (n= 2, 3, 4) and concluded that the limited availability of adsorption sites play an important role for improving the activity. They reported that the stronger binding of one of the *O atoms (after the dissociation of O_2 molecule) will force the other *O atom to migrate towards a weaker binding site, which also forces the OH molecule to adsorb in weaker binding sites, hence reducing the energy required for ORR on the stepped surfaces. As shown in Fig. 3A, the F1 (fcc site down a step) and F2 sites (fcc site next to edge) are the two closest sites for O-adsorption. During the protonation step, both OH species will prefer the most stable E (edge) site. However, the weaker binding of the *O atom at F1 (compared to F2) migrate to the B1 (bridge) site to form *OH (Fig. 3B) due to the repulsion of strongly adsorbed O atom already occupied at the F2 site. Now the two *O atoms are in longer distance and the E site is available. The *O atom of F2 site can now move towards the E site to form OH with higher stability (Fig. 3C). Alternatively, Nørskov and co-workers reported that under the coverage of 1/3 ML OH

(expected coverage under ≈ 0.9V potential), step sites have no role towards destabilizing the reactant intermediates of (111) terrace.[119] These studies imply that the activity of high-index surfaces involves vital local effects which depend on the binding sites, relative positioning of intermediate species and so on which emphasizes the importance of theoretical simulations for activity analysis. Therefore, the exact mechanism providing excellent activity of high-index surface is still unravelled and more detailed studies are required to understand the insights behind the ORR activity on high-index surfaces.
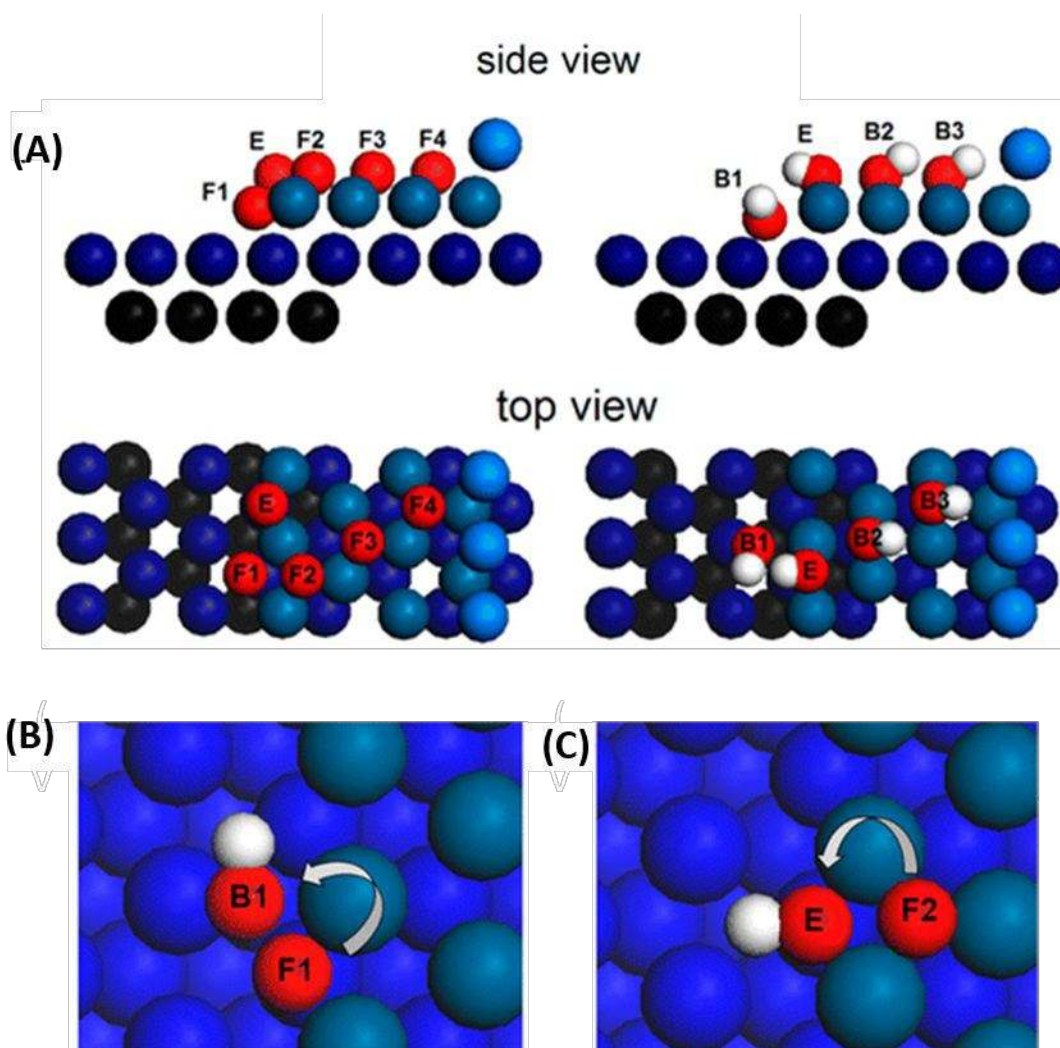
Catalysis Science & Technology Accepted Manuscript

19

Fig. 3: (A) Side and top view of the Pt(221) plane adsorption sites, which consist of oxygen (red), hydrogen (white), and platinum (aqua on the top layer; dark blue on the second layer and black on the bottom layer); Schematic diagram of the protonation reaction (O + H$^+$ → OH) describing the relocation of the (B) O atom on F1 toward B1 site, and (C) O atom on F2 toward E site on the Pt(221) surface. Adapted with permission from ref. 118. Copyright 2015 American Chemical Society.

3.2. Catalysts with less Pt-loading

3.2.1. Pt-based bimetallic catalyst

Alloying Pt with other transition metals is another effective approach for improving the catalytic activity and reducing the Pt-loading as well. Depending on the arrangements of transition metals in the Pt-M (where M = non-Pt transition metal) catalyst surface, it can be classified broadly as: (i) random alloy with a uniform or non-uniform Pt and M distribution; (ii) Pt-skeleton surface and (iii) Pt-skin surface with pure Pt atoms on the top of Pt$_3$M subsurface layers.[120-122]

It is widely accepted that the alloying improves the catalytic performance in two ways, i.e. ligand and strain effect. The ligand effect causes changes in the electronic properties of Pt, which further alters the interaction with the reaction intermediates. The strain effect typically arises due to the size mismatch between the surface and near surface atoms which in turn generates either compressive or tensile strain at the surface layers. The compressive strain downshifts the d-band center, an important activity descriptor describing the weighted average d-states of the metal,[123-126] resulting in a weak adsorption of reaction intermediates, which subsequently improves the catalytic efficiency whereas the tensile strain narrows the d band and shifts d band center close to

the Fermi level and results in a strong adsorption of intermediates. The ligand and strain effects are closely related to each other and often one of them dominates over other. Chen and co-workers[127] demonstrated the effects of alloying towards the ORR catalytic activity in terms of d-band shifts using the Pt (111)-skin surfaces, where the top layer consists of only Pt atoms and the subsurface layer consists of different 3d metals. The subsurface atoms change the electronic structure (d-states) of surface Pt atoms which subsequently changes the adsorption behaviour of the reaction species. The d-band center shifts downwards with respect to the Fermi level when the subsurface layer is chosen further to the left side, which eventually weakens the adsorption of O_2 as depicted in Fig. 4. In contrast, Goddard et al.[128] reported from an experimental study that the universal correlation between d-band center and catalytic activity is not valid. They remarked that ORR activity is linearly correlated with d-band center only when d-band center is linearly related with binding energy. They have further stressed that d-band center model is not applicable when the comparison occurs between different surface plane orientations of the same metal. Xin et al.[129] also offered similar arguments regarding d-band model and reported that the model is not valid when adsorbates have almost completely filled valance shell and the substrates with nearly fully occupied d-band. They illustrated the deviation for the case when OH, F, or Cl adsorbs on metals and alloys characterized by d^9 or d^{10} substrate surface atoms. Therefore, the underlying reason behind the superior ORR catalytic activity of different kinds of catalytic systems is still not clear and is under controversy. Very recently, Back and coworkers have studied ORR activity on Pt-based carbides and nitrides, where the surface layers contain thin Pt overlayers and the underneath layers contain various carbides (CrC, HfC, Mo_2C, NbC, TaC, TiC, VC, WC, ZrC) and nitrides (CrN, HfN, MoN, NbN, TaN, TiN, VN, WN, ZrN).[130] They demonstrated that the conventional catalyst design strategy of tuning the *OH binding energy on

Pt to a weaker binding energy region of the volcano is no longer universal because the scaling

relation between *OH and *O is not preserved due to a strong ligand effect observed in
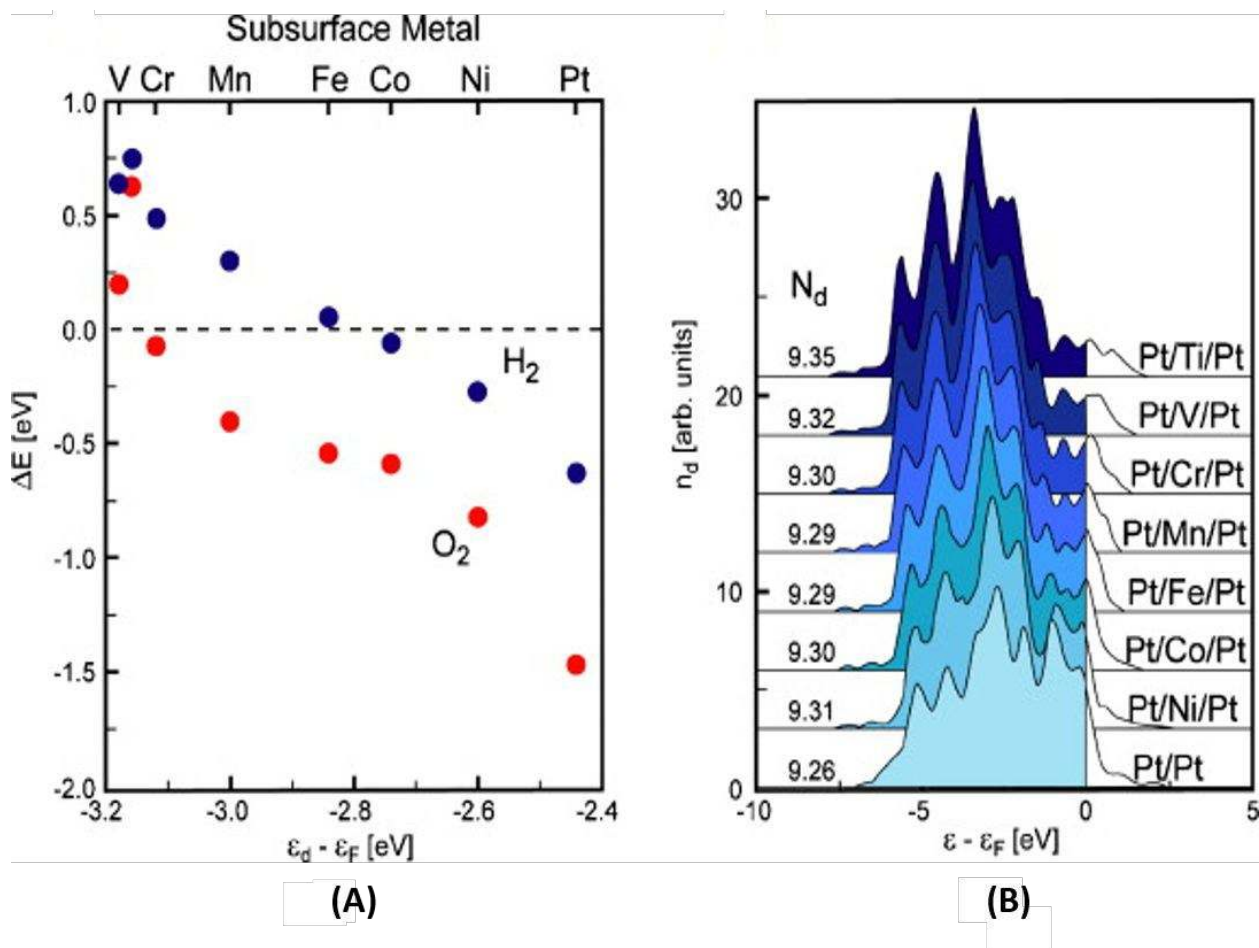
carbide/nitride based structures.

Fig. 4: (A) Adsorption energies of H_2 and O_2 vs. d-band center on different sandwich structures.

(B) The effect of sandwiching a guest metal layer as the first subsurface layer under a Pt surface

on the d-band density of states (DOS) with number of d electrons per surface atom (N_d). Adapted

with permission from ref. 127. Copyright 2015 American Institute of Physics.

Nevertheless, based on the above two approaches (strain effect and ligand effect), there have been a huge number of experimental and theoretical studies regarding the surface modifications of the bimetallic catalysts for improving the catalytic efficiency towards ORR. Breakthrough work by Stamenkovic et al.[131] showed the influence of surface morphology and electronic surface properties on the kinetics of ORR measurements in 0.1M $HClO_4$ at room temperature with 1600 rpm and reported that single crystal surface of Pt_3Ni (111) shows 10 times higher ORR activity than Pt(111) surface and 90 times higher than Pt/C catalysts (Fig. 5A) Three outermost layers of Pt_3Ni(111) basically responsible for the unique properties of the catalyst where the outermost layer consists of 100% Pt, the underneath layer is Ni-enriched with 52% of Ni-contribution and the third layer is Pt-enriched with 87% of Pt-content. Finally, they reported the order of ORR activity as Pt_3Ni (100) < Pt_3Ni (110) < Pt_3Ni (111). The DFT study has shown that Pt-skin surface possess a d-band center of 0.34 eV lower than Pt (111) surface although both the surface possess same surface density of Pt atoms and thus allowing OH species to be adsorbed in low coverage which subsequently increases the number of active sites for O_2 adsorption. Later on, they have carried out extensive investigations on alloy-based bulk PtNi and PtCo surfaces and indicated that the ORR kinetics was dependent on the arrangement of alloying elements on the surface region, reporting the order of catalytic activity as Pt_{bulk} < $Pt_{skeleton}$ < Pt_{skin} surface.[132-135] By combining experimental and theoretical data, Nørskov and collegues[136] have done a screening of Pt_3M alloys and identified the early transition metal alloys especially Pt_3Sc and Pt_3Y showing an activity close to the optimum activity from the volcano plot between activity and oxygen binding energy with only Pt_3Ni(111) ahead (Fig. 5C & D). This observation was further supported by the experimental analysis in which the specific activity of

polycrystalline Pt$_3$Sc and Pt$_3$Y electrodes were enhanced in comparison to pure Pt by a factor of 1.5–1.8 and 6–10, respectively, in a potential range of 0.9–0.87 V.
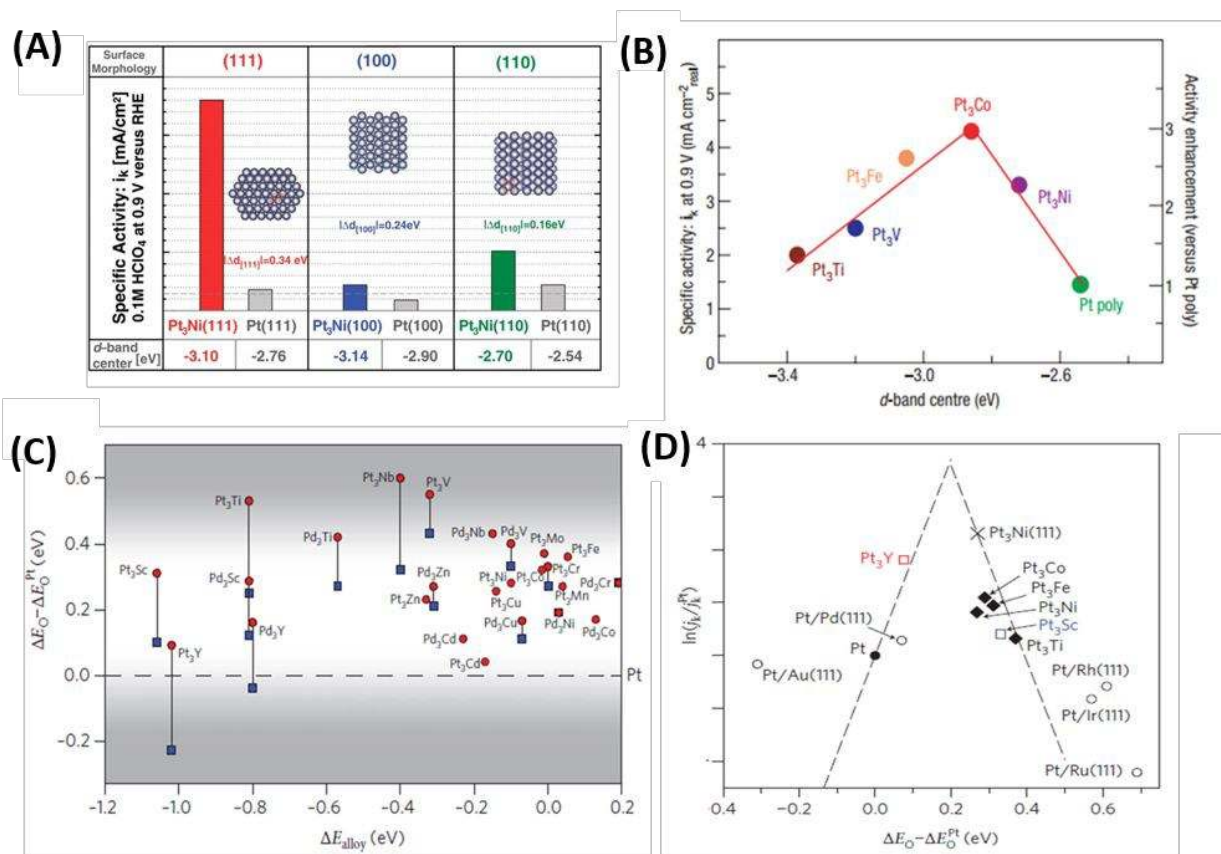

Fig. 5: (A) Kinetic current density i$_k$, measured at 0.9V vs. RHE on various Pt$_3$Ni(hkl) surfaces, in comparison to the corresponding Pt(hkl) surfaces. The horizontal dashed gray line marks the specific activity of polycrystalline Pt. Adapted with permission from ref. 131. Copyright 2007 American Association for the Advancement of Science B) Relationships between experimentally measured specific activity for the ORR on Pt$_3$M surfaces in 0.1 M HClO$_4$ at 333 K Vs d-band center position for the Pt-skin, Adapted with permission from ref. 121. Copyright 2007 Nature Publishing Group C) Output of computational screening procedure, showing the oxygen binding energy, relative to that of Pt, on a Pt or Pd skin surface, as a function of alloying energy and D) Volcano plots for the oxygen reduction reaction on Pt-based transition metal alloys. Measured

kinetic current density as reported in the literature for a range of alloy electrocatalysts with Pt 'skins' plotted as a function of the calculated oxygen adsorption energy. Adapted with permission from ref. 136 Copyright 2009 Nature Publishing Group.

Very recently Pt_5M-based (M= La, Ce, Sm, Gd, Tb, Dy, Tm and Ca) ORR-catalysts have been explored and it was demonstrated that lanthanide contraction can be used to control the strain effects and tune the activity, stability and reactivity of these ORR catalysts.[137] The bulk Pt_5M alloy forms a so-called kagome layer after acid-leaching with a shorter Pt-Pt bond distance (d_{Pt-Pt}) and with a relaxed Pt-overlayer (Fig. 6A & B). The lattice parameter and hence d_{Pt-Pt}, decreased from left to right in the lanthanide series. Fig. 6C is a plot of the ORR activity as a function of the lattice parameter and d_{Pt-Pt}. On the other hand, the binding energy of OH is strongly correlated with d_{Pt-Pt}. Therefore, the alloys on the left of the peak bind OH too weakly, whereas those on the right bind OH too strongly and thus the intermediate Pt_5Tb allows the catalyst to bind OH in optimal range of the Sabatier volcano. The overlayer of lanthanide alloys with a shorter d_{Pt-Pt} than Pt_5Tb could be unstable due to the formation of a more relaxed overlayer. Furthermore, the dissolution potential of different Pt overlayers indicates that the stability decreases as the compressive strain increases (Fig. 6D). This kind of strain-induced destabilization of the Pt overlayer facilitates surface mobility, which in turn provides a channel for the dissolution of any residual lanthanide atoms in close vicinity to the surface and thus decreases the stability.
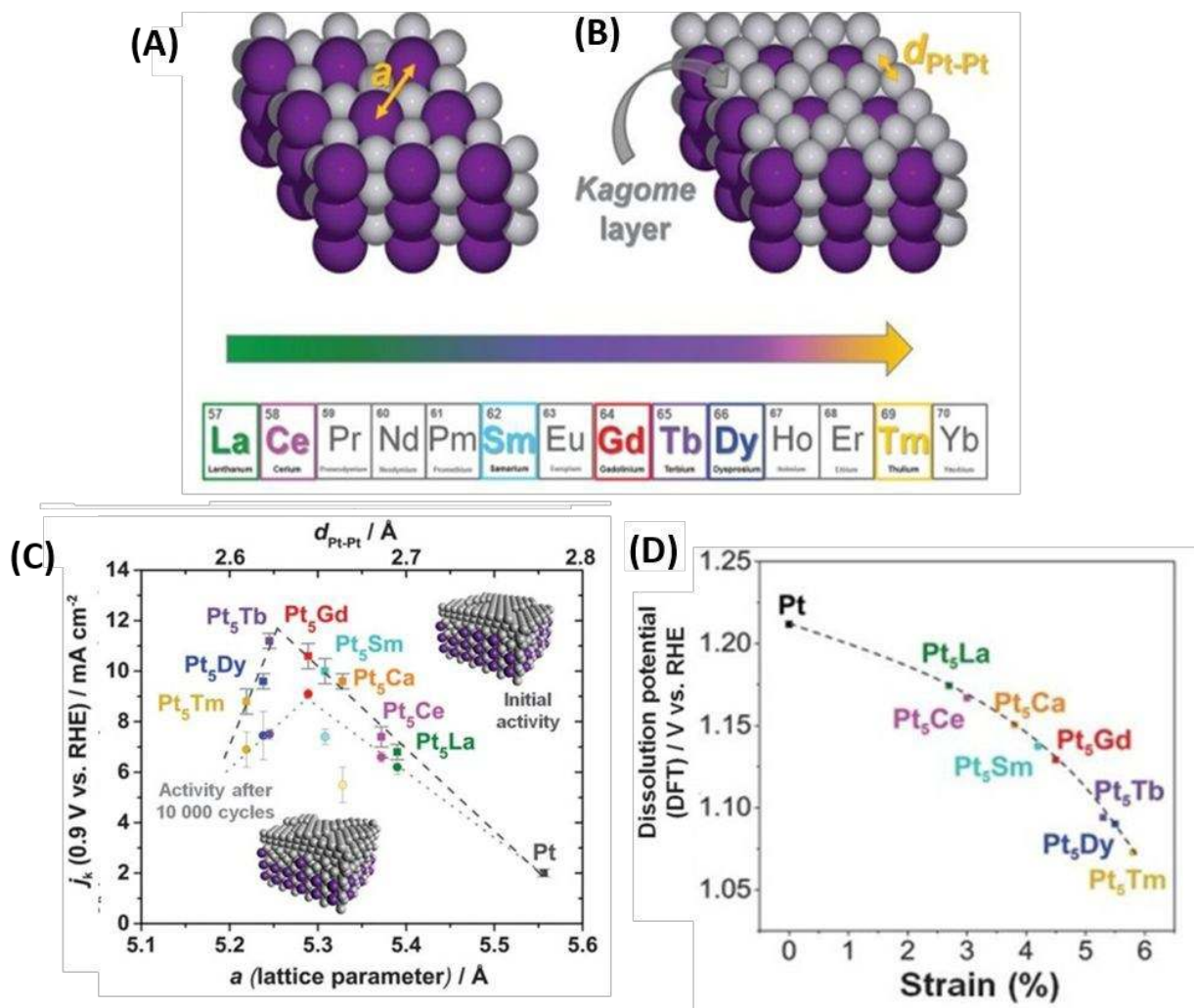
Fig. 6: Schematic view of the bulk structure of a Pt_5M (illustrated for Pt_5Tb), showing Pt_5Tb terminated by (A) Pt and Tb intermixed layer and (B) a Pt kagome layer. Purple spheres represent Tb atoms, and gray spheres represent Pt atoms. (C) Kinetic current density at 0.9 V on polycrystalline Pt_5M electrocatalysts vs. the lattice parameter of bulk Pt_5M (lower axis) and bulk d_{Pt-Pt} (upper axis), respectively. (D) Slab stability represented as dissolution potential vs. the strain of the Pt overlayer on Pt_5M. Adapted with permission from ref. 137. Copyright 2016, American Association for the Advancement of Science.

Aside from bi-metallic alloy, ternary as well as quaternary alloys also have been studied for ORR in recent days. Wang et al. [138] studied ORR on Pt-ternary alloys, $Pt_3(MN)_1$ (M, = Fe, Co and N= Co, Ni) as electrocatalysts and reported that Pt_3CoNi exhibited a higher ORR activity than Pt_3Co and with an improvement factor of $\approx$ 4 compared to the Pt/C. The authors predicted that the employment of ternary Pt-based alloys can serve to additionally tune the oxygen binding energies (weakening of oxygen binding energy compared to Pt(111) surface) of Pt-based catalysts which results in further lowering of barrier for the rate determining step ($O_2(g) + H^+ + e^- + * \rightarrow *OOH$). Apart from ternary alloys, an enhancement in ORR activity and significant durability has been reported for the PtCuCoNi three dimensional nanoporous quaternary alloys by Fu et al.[138] The improvement in activity was explained due to the 3D porous morphology which offers a high porosity and large surface-to-volume ratio as well as the modification of platinum electronic structure owing to the contribution of other elements similar to that observed for the ternary alloys. These studies illustrate that by carefully choosing the nature and composition of non-platinum metals, a subtle progress in reducing the Pt loading and improving ORR activity can be expected.

3.2.2 Core-shell catalysts

While the Pt-alloy catalysts provide excellent ORR activity, the leaching or dissolution of the non-Pt metal from the alloy surface to the acidic solution leads to instability of Pt-bimetallic alloy and hence limits its applicability.[140-142] In this context, the idea of core-shell structure is to reduce the utilization of Pt atoms by depositing a thin Pt-based shell around a non-Pt metal core and thus making a tunable robust layer over the core atoms. Previously, the core-shell nanoparticles have been often theoretically modelled by considering the slab models where the

underneath layers are represented as core layers for the simplicity of calculations.[143,144] But the limitations of slab model for modelling twin boundaries, edge and vertex atoms can be overcome by considering nanocluster model with well-defined facets. The activity differences within different sites of a nanoparticle are mainly originating from the under-coordination, varied interatomic distance and strain generated in these sites which can be better explained from a nanocluster model as compared to a periodic model. Basically, slab model resembles a larger nanoparticle. Therefore, cluster model study with well-defined facet is necessary to simulate the real scenario with respect to the experimental situation. Henkelman and co-workers[145] studied the ORR activity on 2nm M-Au@ Pt nanoclusters M-Ag@Pt (M = Pd, Ir, Rh, Ru, Cu) and provided a linear relationship between the ORR activity and alloy core composition. Based on the oxygen binding energy on the NC's facet, they predicted an optimal composition with $Pd_{105}Au_{35}$@Pt nanoclusters showing highest activity. A linear relation of ORR activity with *O-binding energy on core-shell nanoclusters has been reported and suggested that the 3d-metal as core atoms for good catalytic activity.[146,147] Jennings et al.[148-150] calculated the O_2 dissociation reaction on the various possible sites of the Pt_{79} NC's facets and proposed that the late d metals from group 9-12 which interacts weakly with the Pt shell, will be beneficial for the O_2 dissociation reaction. Nevertheless, complete ORR pathway on the nanocluster surface sites has not been scrutinized for long time. Our group have studied complete ORR pathway on Ti_{19}@Pt_{60} cuboctahedral core-shell nanocluster.[45] We demonstrated that the *O_2-induced structural changes favour direct *O_2 dissociation over the Ti_{19}@Pt_{60} NC despite the presence of tensile strain on the surface atoms. The observation was completely opposite from previous reports on alloy-based catalysts, where the compressive strain generated at the surface layer due to alloying (Strain effect) was credited for their superior catalytic activity. Furthermore, we revealed that a dual mechanism (ligand

effect and charge transfer) plays an important role to improve the ORR on the $Ti_{19}@Pt_{60}$ NC, where the ligand effect favours reaction thermodynamics, whereas charge accumulation on the *O atom improves the reaction kinetics.

Huang et al.[151] have reported in a combined theoretical and experimental study, a new class of catalysts in the framework of Pt_3Ni configuration. They have doped various transition metals like vanadium, chromium, manganese, iron, cobalt, molybdenum (Mo), tungsten, or rhenium on the Pt_3Ni octahedral nanoclusters. The Mo-Pt_3Ni/C showed the best ORR performance, with a specific activity of 10.3 mA/cm^2 and mass activity of 6.98 A/mg$_{Pt}$, which are 81- and 73-fold enhancements compared with the commercial Pt/C catalyst (0.127 mA/cm^2 and 0.096 A/mg$_{Pt}$) by Alfa Aesar, 20 wt. % Pt, Pt particle size: 2-5 nm, as has been used by the authors. Notably, Tanaka commercial Pt/C catalysis shows a mass activity of 0.42 A/mg$_{Pt}$.[152] However, using cluster expansion method for Pt-Ni-Mo NCs in Monte Carlo simulations, the authors identified that the equilibrium structures possesses a Pt skin, with Mo atoms preferring sites in the second atomic layer along the edges connecting two different (111) facets (Fig. 7A & B) in vacuum. The cluster expansion method considers a series of many body interactions (known as effective cluster interactions) over a number of site variables along with fitting to the data obtained from first principle calculations to address the configurational problems in alloys.[153,154] Further, DFT calculations also indicated that the Mo prefers to stay at subsurface site compared to surface site in vacuum, but in oxidizing conditions, Mo tends to segregate to the surface vertex/edge sites (Fig. 7C). Mo doped structures improve the stability in two ways. Firstly, the Mo-oxide species at the surface replace the surface Ni atoms. Secondly, the dissolution of Ni and Pt atoms get suppressed due to the formation of relatively strong Mo-Pt and Mo-Ni bonds. Authors reported that Mo on an edge or vertex site increases the energy required to remove a Pt atom from a

neighbouring edge or vertex site by an average of 362 meV, and to remove a Ni atom by an average of 201 meV. Authors suggested that the O-atom binding energies in the doped NC near the Mo atoms are decreased by up to 154 meV, whereas it binds too strongly in the undoped system (Fig. 7D & E). As a result, edge sites along with the (111) facet becomes highly active for catalysis. On their later work, Huang and co-workers,[155] combining *in situ* and *ex situ* electrochemical and synchrotron-based X-ray absorption spectroscopic (XAS) studies, density functional theory calculations, and kinetic Monte Carlo model, investigated the specific role of Mo-doping on PtNi/C octahedral nanoparticles and reported that the existence of surface Mo-oxides at the vertex and edge sites of Mo−PtNi/C octahedral NPs stabilizes the adjacent under-coordinated Pt sites, which stabilize the octahedral shape enriched with (111) facets Pt sites. This stabilization of (111) facets eventually lead to increased concentrations of Ni in subsurface layers where they get protected from acid medium. As a result, the desired $Pt_3Ni(111)$-like near-surface structure is stabilized in acidic media throughout the entire fuel cell operating potential range against voltage cycling. Along with these indirect promoting effects, the increased concentration of Ni in the Mo−PtNi/C NPs directly improves the ORR kinetics by reducing the binding energies of oxygen containing adsorbates, following the d-band center model. In the context of doped PtNi/C NPs, Beermann et al.[156] presented Rh-doped Pt−Ni octahedral NPs with mass activity of 1.14 A/mg_{Pt} along with the shape stability compared to the bimetallic Pt−Ni octahedral counterpart. From the microstructural investigations of the atomic rearrangement processes on the surfaces of the two types of catalysts, authors found that the shape losses in Pt-Ni NPs occur mainly due to the Pt atom diffusion during dynamic potential cycling, while Rh mainly locating at the surface of the particles, suppresses the diffusion of Pt at the edges and kinks maintaining a stable shape and active surface structures of the doped NPs.
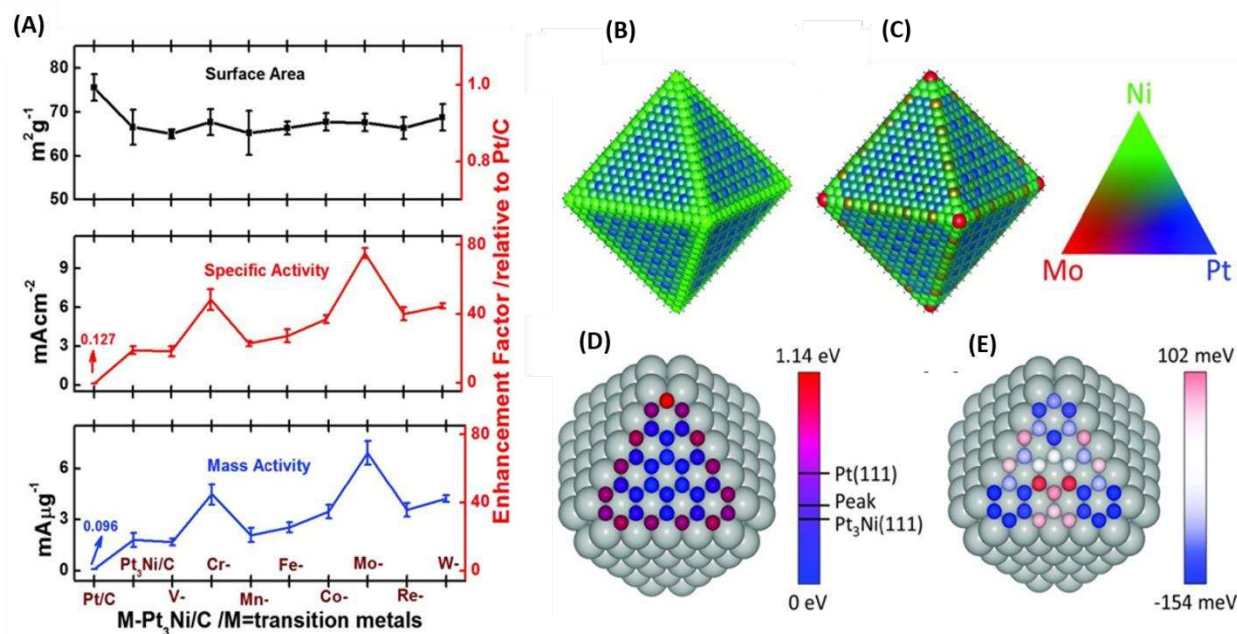
Fig. 7: (A) The electrochemically active surface area (top), specific activity (middle), and mass activity (bottom) at 0.9 V vs. RHE for different transition metal–doped Pt_3Ni/C catalysts. The average site occupancies of the second layer of (B) the $Ni_{1175}Pt_{3398}$ NC and (C) the $Mo_{73}Ni_{1143}Pt_{3357}$ NC indicated by the color triangle (D) The calculated binding energies for a single oxygen atom on all fcc and hcp sites on the (111) facet of the $Mo_6Ni_{41}Pt_{178}$ NC, relative to the lowest binding energy, where the gray spheres represent Pt, and colored spheres represent oxygen sites. (E) The change in binding energies when a $Ni_{47}Pt_{178}$ NC is transformed to a $Mo_6Ni_{41}Pt_{178}$ NC by the substitution of Mo on its energetically favored sites in the second layer below the vertices. Adapted with permission from ref. 151. Copyright 2015 American Association for the Advancement of Science.

However, the segregation of inside core atoms towards outside layer in a core shell nanocluster is also a matter of concern. Wang and Johnson[157] have performed a detailed theoretical study on 55-atom based cuboctahedral nanocluster alloys of late transition metals by considering

segregation energy as an important parameter. They reported that the core-shell preferences from the segregation energies are described largely by only two independent key factors i.e, the cohesive energy and the Wigner-Seitz radius (atomic size) and also the interplay between them. For core-shell nanoparticles formed between atoms from different groups, the metal with the largest cohesive energy prefers to stay in the core. For core-shell nanoparticles formed by atoms within a group, the metal with the smallest atomic size goes into the core. As has been shown in Fig. 8A, the Pt prefers to remain as shell atoms when the Ni, Ir, Rh, Co, Os, Ru and Fe are used a core metals, whereas Pt prefers to stay as core atoms in case of Au, Ag, Cu and Pd metals. In our recent study[158], we reported that Au@Pt is not favourable, whereas Co@Pt is favourable. However, the unfavourable nature of Au@Pt decreases with increasing concentration of Co@Pt in an $Au_{10}Co_9@Pt_{60}$ trimetallic cluster. In contrast, Henkelmann and co-workers reported that Au@Pt, Ag@Pt, Ir@Pt and Rh@Pt are stable in both vacuum and oxidizing environment.[145] Pd@Pt and Ru@Pt are stable only in bare form but unstable in presence of oxidizing environment. It is noteworthy to mention that the extent of stability of the nanoclusters changes from bare nanoclusters to O-adsorbed nanoclusters, which is in agreement with the study by Wang et al.
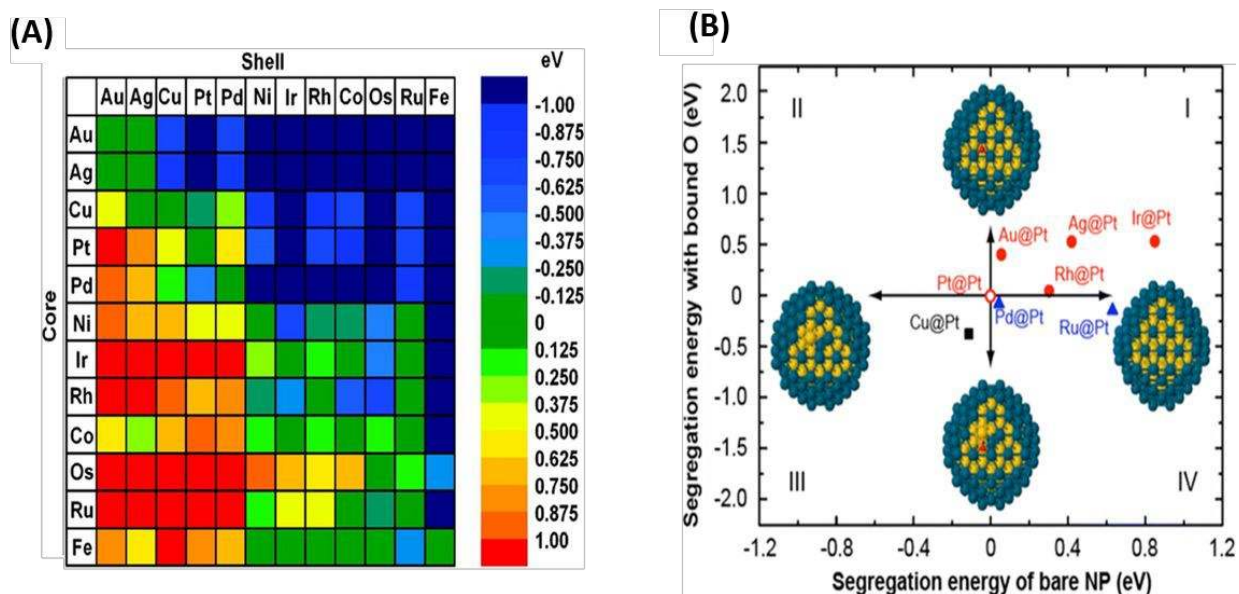
Fig. 8: A) Color-coded matrix of DFT-PW91 segregation energies for impurity in 55-atom nanoparticle composed of 12 late-transition metals (132binaries). Adapted with permission from ref. 157. Copyright 2009 American Chemical Society (B) stability of Pt-shell particles based on the segregation energy with and without adsorbed oxygen for various core-shell nanoparticles. The insets indicate the stable structures along each axial direction. Adapted with permission from ref. 145. Copyright 2013 American Chemical Society

3.2.3. Hollow nanostructured catalysts

Hollow nanostructures have been emerged as very promising catalysts due to their excellent ORR activity and less Pt-loading. Several studies on Pt_3Ni hollow structures with excellent ORR activity have been reported recently. Chen et al.[159] reported an enhanced ORR performance of Pt (111)-skin based Pt_3Ni nanoframes (Fig. 9) which exhibits an enhancement by 16-fold in specific activity and 22-fold in mass activity compared to the commercial Pt/C catalysts. The high specific activity of the Pt_3Ni nanoframes arise from the formation of the two mono-layered thick Pt-skin surface on the nanoframes, as well as the open structure of the Pt_3Ni nanoframes that

allows access of the reactant molecules to both the internal and external surface atoms. Very

recently, Wang and coworkers[160] synthesized Pt_3Ni alloy tetrahexahedral(THH) nanoframes with

high-index facets [(310), (410), (510) and (720)]. The authors have found in their DFT study that

the segregated Pt thin layer is under compressive strain, which results a down-shift of the d-band

center which attributes the lowering the binding strength of the reaction intermediates in the

catalytic process. The Pt_3Ni THH nanoframes exhibit 8 times higher specific activity and 5 times

higher mass activity compared to Pt/C in ORR activity. Using X-ray absorption spectroscopy,

Becknell et al.[161] also reported the importance of Pt-atom segregation at the surface for Pt_3Ni

nanoframes for improving the ORR efficiency. They reported that insufficient segregation of Pt

atom in the surface forms a rough and thin Pt layer, resulting in the strong binding of the

adsorbates. In contrast, well-segregated Pt layer over the Ni-rich subsurface layers binds the

intermediates weakly, which results an improved ORR activity. Therefore, the high ORR activity

of the Pt_3Ni hollow nanoframes strongly depends on the formation of Pt-skin surface structure.
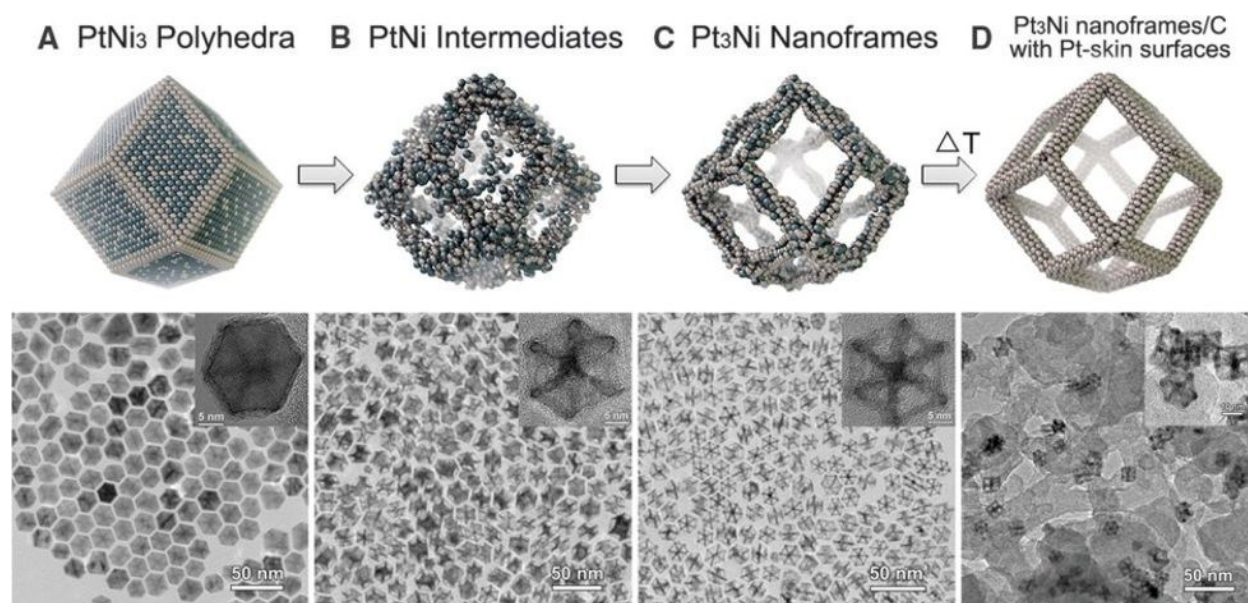

Fig. 9: Schematic illustrations and corresponding TEM images during the evolution process from polyhedra to nanoframes. (A) Initial solid $PtNi_3$ polyhedra. (B) PtNi intermediates. (C)

Catalysis Science & Technology Accepted Manuscript

Final hollow Pt_3Ni nanoframes. (D) Annealed Pt_3Ni nanoframes with Pt(111)-skin–like surfaces dispersed on high–surface area carbon. Adapted with permission from ref. 159. Copyright 2015 American Association for the Advancement of Science.

Apart from Pt_3Ni based nanocage, researchers have been able to synthesize pure Pt-based nanocage with excellent ORR activity. Xia and coworkers[162] synthesized cubic and octahedral nanocages by depositing a few atomic layers (seven atomic layers) of Pt on Pd nanoparticles with well-defined facets and followed by etching away the Pd templates (Fig.10A & B). The octahedral nanocages exhibited a specific activity of 1.98 mA/ cm^2 with the mass activity of mass activity of 0.75 A/mg_{Pt} at 0.9 V_{RHE}. The authors credited the lower Pt-Pt bond distances (2.76 – 2.80 Å) for improved energetics of the rate determining steps. They suggested that the etching process is initiated by oxidizing the Pd atoms in the outmost layer of the Pt shell to generate surface vacancies, followed by diffusion of Pd atoms from underlying layers to generate more vacancies. This diffusion process undergoes through combination of two pathways (Fig. 10C). In the hopping mechanism, Pd adatoms diffuse across the Pd (100) surface with an activation barrier of 0.99 eV. In the substitution mechanism, the Pt adatom can substitute into the Pd surface, pushing the Pd atom to a nearby hollow surface site with an activation barrier of just 0.74 eV. In the combination of these two mechanisms, some Pd atoms will be incorporated into the Pt shell and eventually Pt overlayer is formed. However, the activation energy barrier for Pt substitution increases as the Pt coverage increases and therefore, the substitution of all the Pd atoms becomes kinetically unfavorable. Nevertheless, Pd atoms were incorporated into the Pt shell through a co-reduction mechanism at the later stage of etching process. Later on, the same group reported Pt-based icosahedral nanocages with a specific activity of 3.50 mA/ cm^2 toward

ORR, much greater than those of their earlier report of 1.98 mA/cm^2 on Pt-based octahedral nanocages.[163] The presence of twin boundaries along with (111) facets on the surface is responsible for the improved ORR activity.
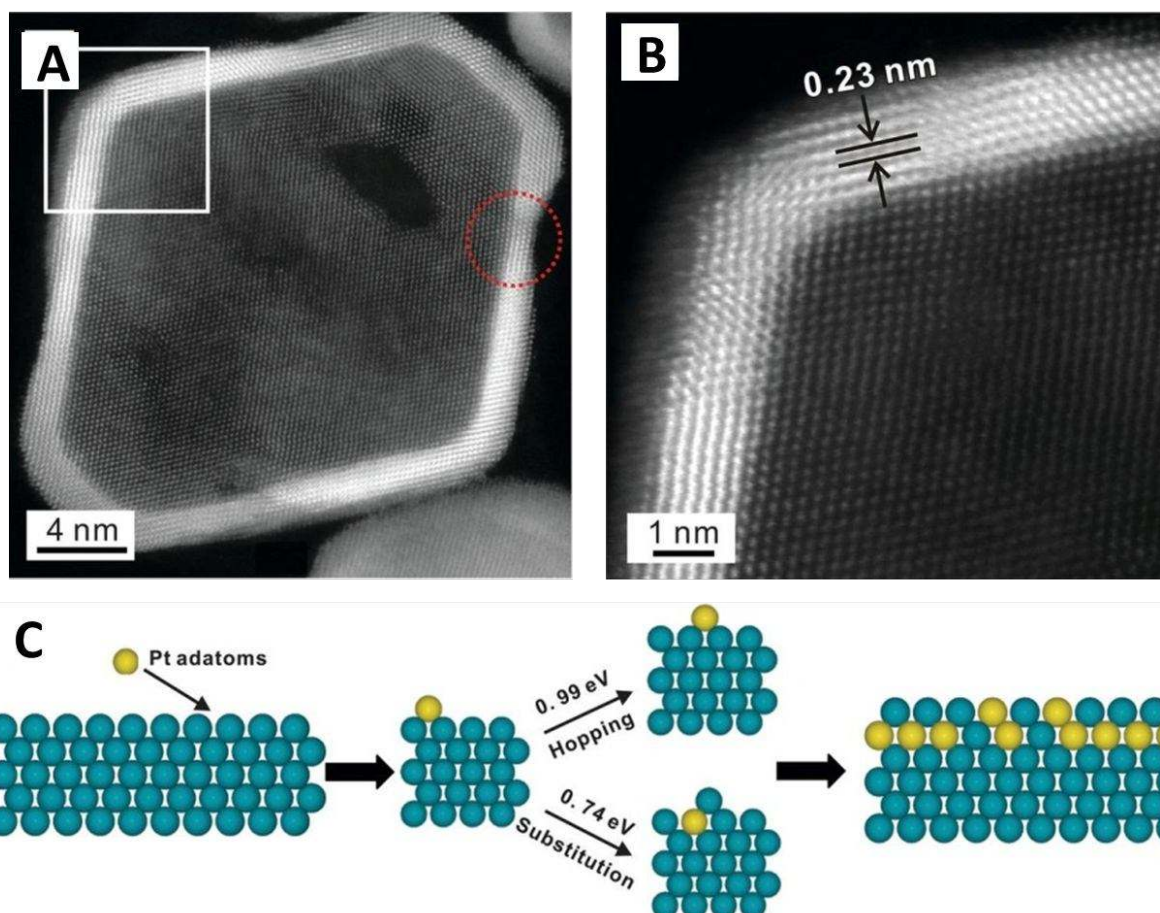

Fig. 10: (A) HAADF-STEM image of a nanocage. (B) High-resolution HAADF-STEM image taken from the region boxed showing a wall thickness of seven atomic layers. The red circle represents the hole causing the dissolution of Pd from the core (C) Mechanistic details for the deposition process with DFT calculated activation barriers. Adapted with permission from ref. 162. Copyright 2014 American Association for the Advancement of Science.

Inspired by these experimental successes on few-layered hollow structures, our group has modelled a single layered octahedral nanocage based on the octahedral geometry to check how

single layered structure influences ORR as depicted in Fig.11.[144] We found that single layered

hollow nanocage is highly strained elevating the ORR activity. More importantly, we found that

the charge transfer towards the adsorbed oxygen atom is higher in case of nanocage structure

compared to the bulk Pt(111) surface, which helps to easy protonation to form adsorbed *OH

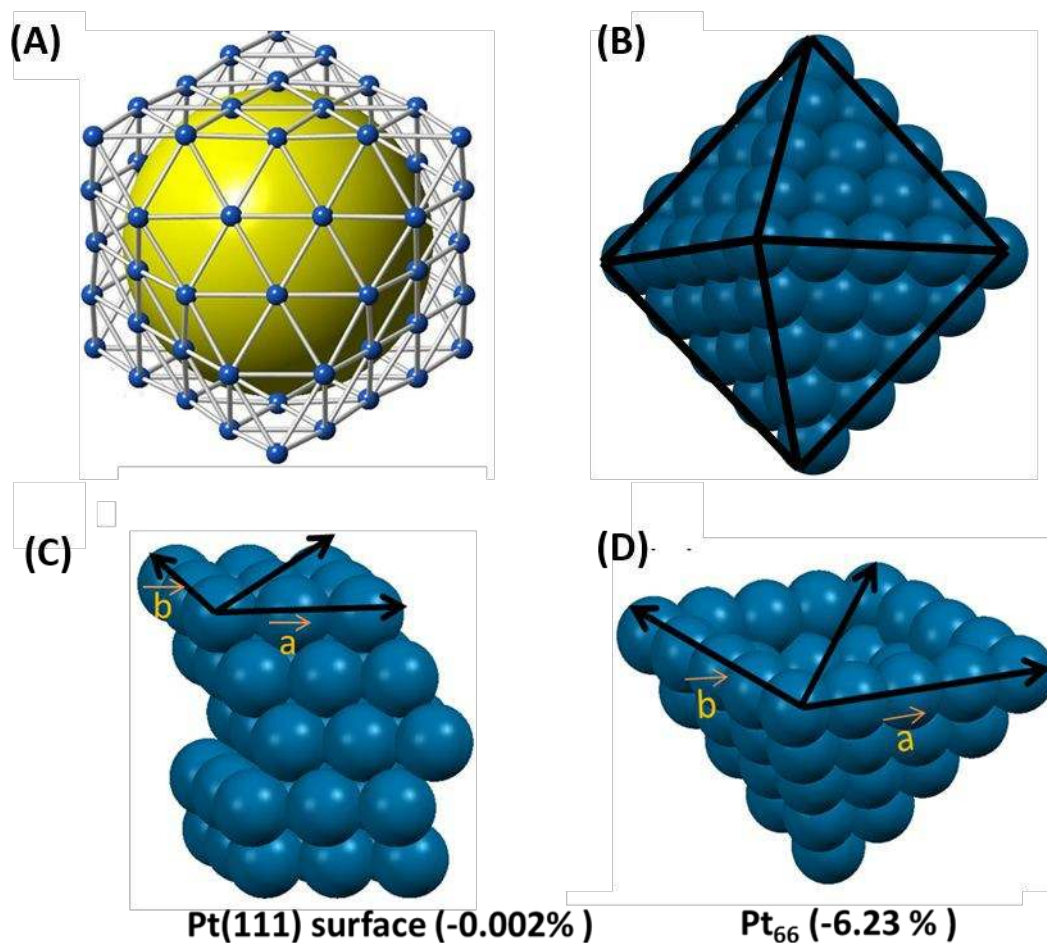and lowers the activation barriers of the elementary steps.

Fig. 11: (A & B) Octahedral nanocage with eight (111) facets; the yellow sphere represents the

inside void of the nanocage. The compressive surface strain on (C) the bulk Pt (111) and (D)

nanocage. Adapted with permission from ref. 164. Copyright 2016 Royal Society of Chemistry.

3.2.4 Nanosheet and Nanowire catalysts

Since the discovery of graphene, two-dimensional (2D) materials with an atomic layer thickness have attracted widespread attention due to a number of unusual properties and potential applications in next-generation devices in the fields of electronics,[165-167] optics,[168,169] magnetism[170,171] and catalysis[172-175]. Although metal atoms have a strong preference towards three-dimensional (3D) close-packed structures, recent experimental realization of metal nanosheets of Pd (1.8 nm)[176], Rh (1.3 nm) [177] and Ru (1.5 nm)[178] have shown a direction in the area of ultrathin metal nanosheets. Huang and co-workers[179] have synthesized platinum-lead/platinum (PtPb/Pt) core/shell nanoplate as ORR catalyst and reported the specific and mass activities of 7.8 mA/cm^2 and 4.3 A/mg$_{Pt}$ at 0.9 V vs. RHE, respectively. Pt shell thickness of the nanoplate was determined to be about 0.8 to 1.2 nm (four to six atomic layers) possessing the Pt(110) facet at the outside shell layers (Fig. 12). It is typically accepted that the low-coordinated sites bind O-atom very strongly and hence lower the ORR performance. However, their DFT study revealed that the large tensile strain generated at the Pt-shell layer helps to reach the O-atom binding energy towards optimal range even in the catalytically unfavorable low-coordinated bridge sites and thus improve the overall ORR activity. This observation owes significant attention as it evidences the dominance of site dependence over the generally accepted strain effect in determining the ORR activity.
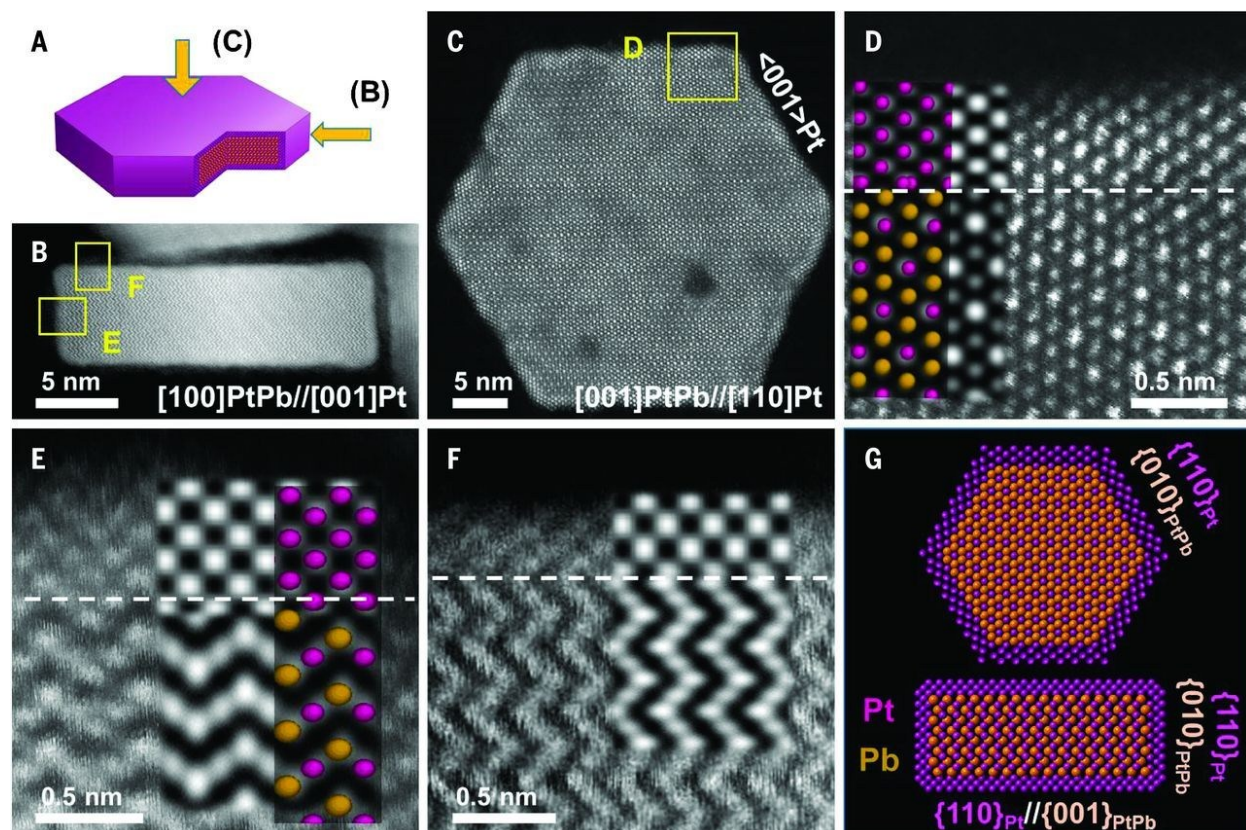
Fig. 12: (A) A model of one single hexagonal nanoplate, (B) HAADF-STEM image along PtPb[100] zone axis, (C) HAADF-STEM image PtPb[001] zone axis. (D) is a high-resolution HAADF image from the selected area in (C) represented by yellow rectangle. (E) and (F) are high-resolution HAADF images from the selected areas in (B) represented by yellow rectangles. Simulated HAADF images as well as the atomic models are superimposed on the experimental images. (G) The schematic atom models of the nanoplate showing the top interface [(110)Pt//(100)PtPb] and the side interface [(110)Pt//(001)PtPb]. Adapted with permission from ref. 179. Copyright 2016, American Association for the Advancement of Science.

In our recent study,[31] we have predicted a singled-layered platinum sheet (Fig. 13A & B) with an orthorhombic buckled (110) surface which has shown enhanced ORR activity. A stability comparison has shown that the buckled (110) Pt sheet owns more stability than any of the (111)

or (100) sheets as well as the planar (110) sheet. Although it is generally accepted that Pt (111) surface has more ORR activity than Pt (110) surface, the aforementioned work from Huang's group[179] with (110) nanoplates resulting superior activity reported during the same period validated our structural as well as activity prediction of a Pt (110) nanosheet. We demonstrated that the d_{z2} orbitals of the out-of-plane Pt atoms tilt themselves (by 30°) toward the d_{yz} orbital of the in-plane Pt atoms to gain the maximum overlap, which in turn stabilizes the buckled structure (Fig. 13C). Furthermore, we showed that an orbital mixing between an in-plane s-orbital and out-of-plane p-orbital helps in stabilizing the buckling pattern (Fig. 13D). Our calculated reaction barrier study revealed that OH formation step becomes highly favourable on this single-layered structure and we attributed unique adsorption behaviour of O-atom on the platinum monlayer as underlying reason. The similar adsorption sites of both *O and *OH on the monolayer makes the OH formation step favourable on it (Fig. 13F&G).
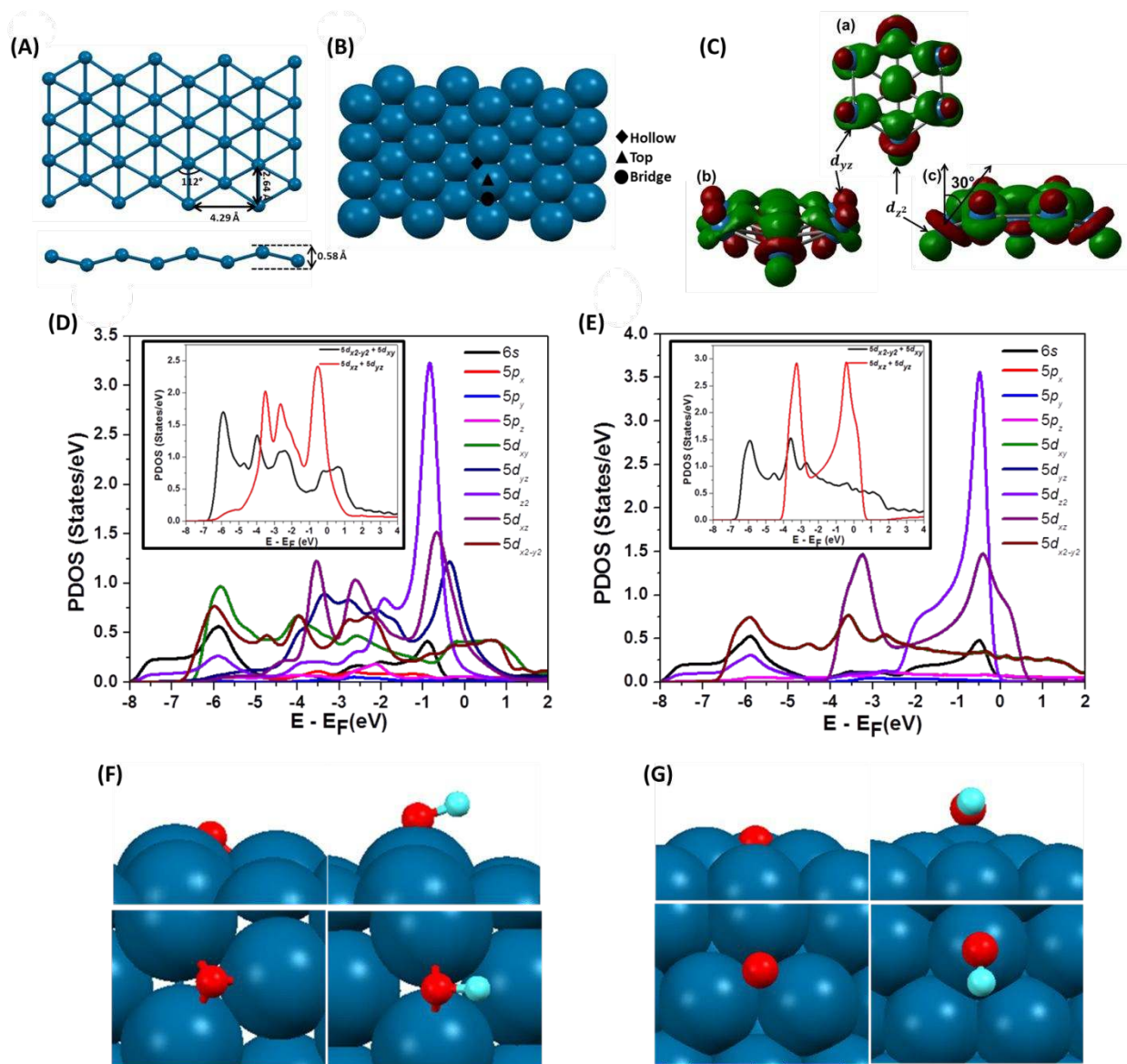
Fig. 13: (A) Structural parameters and (B) adsorption sites on platene; (C) orbital compatibility of buckled Pt₇ cluster; projected density of states (PDOS) of (D) platene and (E) planar platinum structure; adsorption pattern of adsorbed O and OH on (F) platene and (G) periodic Pt(111) surface. Adapted with permission from ref. 31. Copyright Royal Society of chemistry.

Another category of nanocatalysts, which have attained immense attention in the recent decades, are one dimensional metal nanostructures such as nanowires (NWs), nanotubes(NTs) and

nanorods. Their noticeable catalytic activity stems from morphological aspects especially the unique anisotropic structure, low defect density and less platinum agglomeration problem.[180-183] Guo and cowrkers[184] have nicely reviewed the synthetic strategies for tuning platinum nanowires and nanotubes for fuel cell applications. Pt-based nanowires with sub-nanometer thick walls have been reported by Jiang et al.[185] They synthesized sub-nanometer sized monometallic and alloy (PtNi, PtCo and PtNiCo) based Pt NWs with a diameter of only 4 to 5 atomic layer thickness showing exceptional mass and specific activities of 4.20 A/mg_{Pt} and 5.11 mA/cm^2 at 0.9 V vs. RHE. Through DFT studies, the authors credited an optimal binding energy of O-atom (lower by 0.2 eV than Pt (111) surface) at the hollow fcc site of (111) facet of the NWs for higher ORR activity. They further demonstrated that the compressive strain generated at the surface of the (111) facet of the NWs is the underlying reason for lowering the binding energy of O-atom (Fig. 14A, B & C). Very recently, Li et al.[186] have synthesized jagged Pt nanowires (J-Pt NW) (Figure 15A) exhibiting an electrochemically active surface area of 118 m^2/g_{Pt} and a specific activity of 11.5 mA/cm^2 for ORR (at 0.9 V vs. RHE), yielding a mass activity of 13.6 A/mg_{Pt} (Fig. 15B). From reactive molecular dynamics simulations, the authors have suggested that the highly stressed, under-coordinated rhombus-rich surface configurations of the jagged nanowires enhance ORR activity while comparing with more relaxed surfaces. They reported that the coordination number (evaluated by counting all neighbors within a distance cut-off of 3.0 Å) of surface atoms in the J-Pt NWs ranges mostly between 6 and 8 (Fig.15C), compared to typical crystal surfaces like Pt(100) and Pt(111), where the coordination numbers are 8 or 9 for, respectively. Interestingly, the J-Pt NWs possess crystalline-like character of surface atoms despite the low coordination number and jagged features. The authors have further reported that the distribution of most of the rhombus dihedral angles (defined by the angle formed between the

two lines connecting atom 1 and 2 to the middle point of atoms 3, 4 respectively as highlighted by the yellow arrows in the inset) (Fig. 15D) lies in the range of 156° to 180°, whereas the dihedral angle for typical crystalline Pt (111) facets is 180°. Most of the angles are between 156° and 180°, which suggest that the surfaces of the J-Pt NWs are highly comparable typical crystalline structure. The high-crystallinity nature of the J-Pt NWs is one of the underlying reasons for increased reactivity.
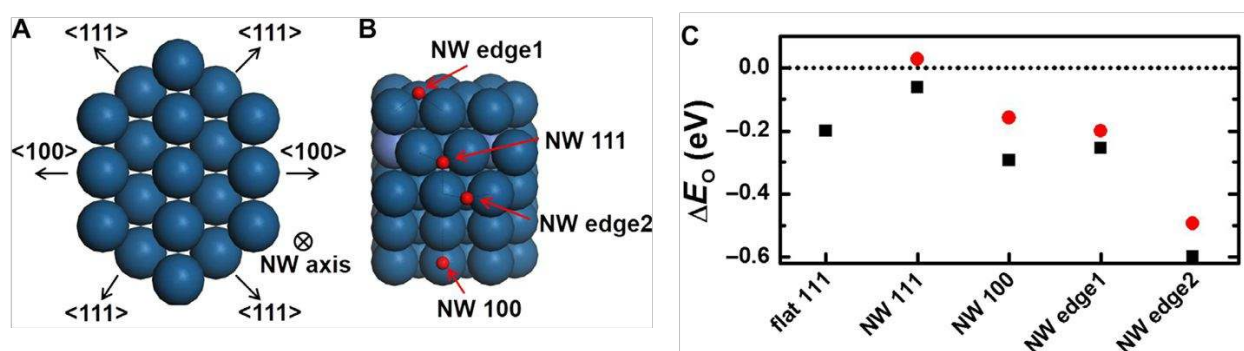

Fig. 14: A) Modelled single crystalline Pt nanowire with four (111) facets and two (100) facets. B) Stable adsorption sites for O on the NW surface. C) O adsorption energy of on Pt (111) surface (black squres) and Pt-based NWs (red circles). Adapted with permission from ref. 185. Copyright 2016 American Association for the Advancement of Science.
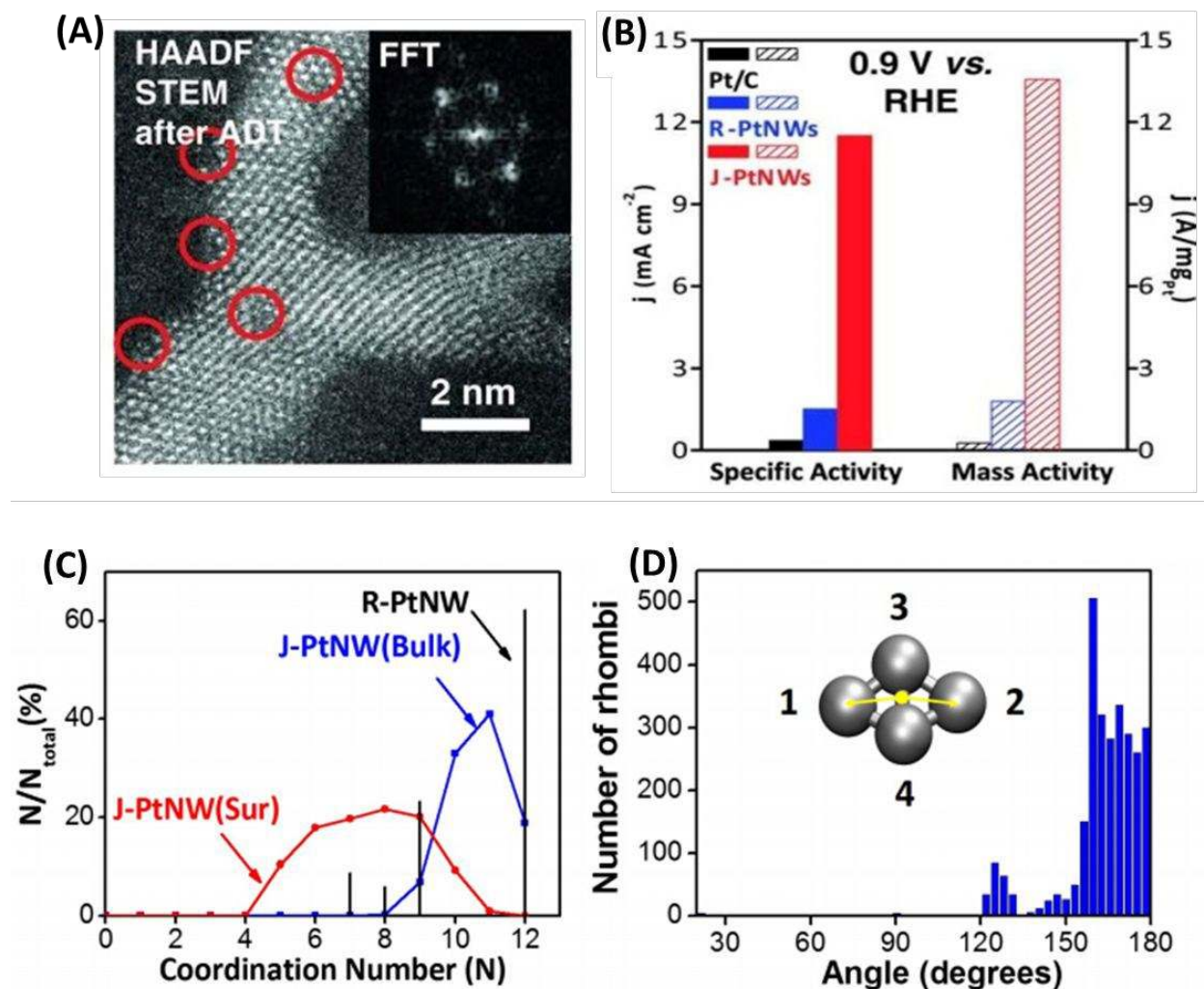
Fig. 15: (A) High-resolution HAADF-STEM image of the J-Pt NWs. The red circled areas indicate defective regions with missing atoms and the inset shows the corresponding FFT image. (B) Comparison of specific activities and mass activities of the J-Pt NWs, synthesized regular Pt NWs (R-Pt NWs) and Pt/C catalyst at 0.9 V versus RHE. (C) Coordination number for surface atoms (red) and bulk atoms (blue) of the J-Pt NWs and R-Pt NWs (black). (D) Schematic depiction of a rhombus (inset) and the distribution of the dihedral angle between the two triangles of the rhombus. Adapted with permission from ref. 186. Copyright 2016, American Association for the Advancement of Science.

In addition to nanowires, platinum based nanorods and nanotubes have also explored for their catalytic activity towards ORR. A subtle amount of information regarding the structural dependent activity of these nanostructures has been gained from first principle studies very recently. With the aid of catalyst models which can incorporate the relative aspect ratio, arrangement of facets, boundaries and chemical composition, the origin of enhanced activity of one dimensional nanostructures has been unravelled. By modelling a nanorod with both (111) and (100) facets separated by edges, Gambu et al.[187] observed a localized edge effect which provides a kinetic connection between (111) and (100) facets through O transportation which is more pronounced at high coverage. They have also predicted that a high *O coverage is thermodynamically favourable at the edge sites. A density functional study of ORR activity of single walled platinum nanotubes of various diameters by Matanovic et al.[188] have observed a dependence of catalytic activity and stability toward electrochemical dissolution on the diameter and chirality of the nanotube. From this study, the authors suggested that platinum nanotubes with a diameter greater than 1nm could be useful as potential catalysts for ORR as they have observed to possess an overpotential value close to bulk platinum. Recently, our group has also modelled a multi-layered platinum nanotube with (111) and (100) facets and analyzed the ORR activity and selectivity.[189] The nanotube has been found to be highly selective towards four-electron reduction pathway with O protonation as the rate determining step. A similar extent of ORR activity was observed for both (111) facet and edge sites with a slightly reduced overpotential than bulk platinum. These studies proclaim the plausibility of achieving sound improvement in ORR catalysis by carrying out studies scrutinizing the structural and shape dependent activity of one dimensional nanostructures.

3.2.5. Single-atom Catalysts

In spite of being addressed to a limited extent, Pt based single atom catalysts (Pt-SACs) as well as a few atom catalysts are another excellent choices for fuel cell catalysis as they are associated with a maximum reduction of platinum loading. They have been found to exhibit pronounced catalytic activity for electrochemical reactions.[190-193] Liu et al.[194] have studied the ORR activity of BP (Black-Perals) 2000 carbon-supported doped-N triggered Pt-SAC (Pt1-N/BP) and compared with a pure carbon supported Pt SAC (Pt1/BP) and pure N-doped carbon (N/BP). The higher half wave potential ($E_{1/2}$ = 0.76V) obtained for Pt1-N/BP from the rotating ring-disk electrode (RRDE) experiment in comparison with N/BP ($E_{1/2}$ = 0.51V) and Pt/BP ($E_{1/2}$ = 0.44V) implied a synergetic effect between doped-N and Pt single atoms which causes an enhancement in ORR activity which is observed in both acidic and alkaline media (Fig. 16A). The improved durability and activity of Pt1-N/BP was explained by the stronger adsorption of Pt atom on N doped graphene surface (g-P-N1-Pt1) and its higher binding of O_2 respectively in comparison to pristine graphene surface devoid of Pt (g-P-N1). The DFT catalytic cycle study also remarked a lower overpotential on g-P-N1-Pt1 supported the experimental observation as compared to g-P-N1, which further supports the experimental observations (Fig. 16B). In a theoretical screening study of single metal atoms anchored in two-dimensional materials, Back et al.[195] reported that the d-states in Pt-SACs are much more localized than Pt (111) which could alter the conventional scaling behaviour between *OOH and *OH which can be expected to tackle the overpotential problem. Analogous to SAC, 4 to 6 atom platinum nanorafts formed on disordered Mo_2C support has been reported to perform as efficient catalysts for ORR from a DFT study by Krishnamurthy et al.[176] The disordered structure of Mo_2C as well as interaction of nanoraft atoms with H_2O provides an alternative scaling between ORR intermediates and an ORR onset potential of 0.6 V

closer to 0.75 V for Pt (111) indicating a similar catalytic activity as that of platinum bulk surface. Therefore single or a few Pt atoms based catalysts are expected to contribute significantly to the burgeoning research for developing highly efficient fuel cell catalysts.
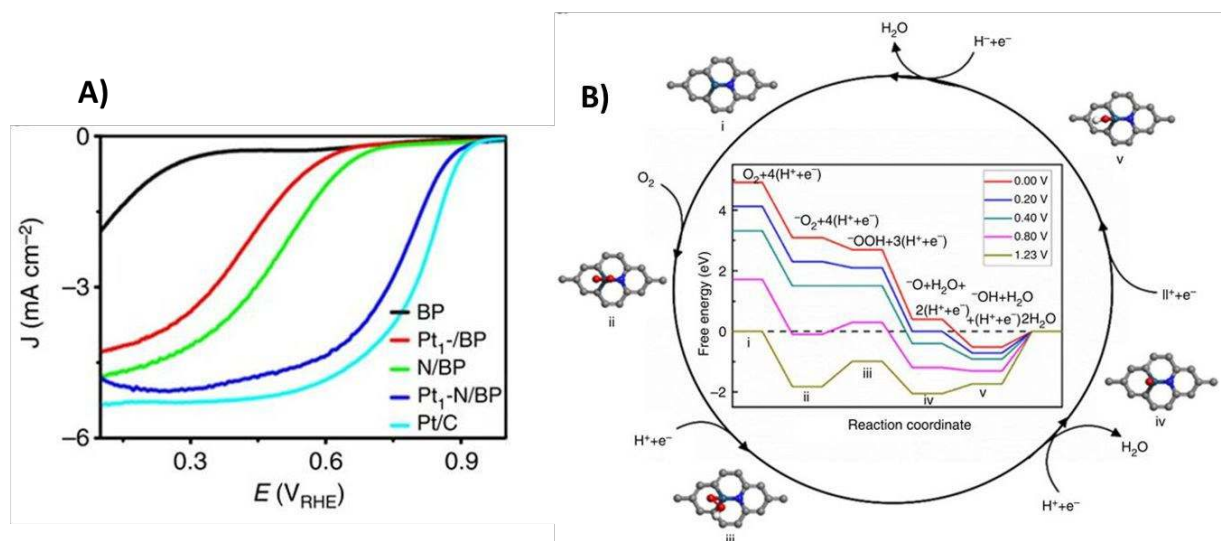

Fig. 16: A) RRDE polarization curves of BP, N/BP, Pt1/BP, Pt1-N/BP and commercial Pt/C in O_2-saturated 0.1M HClO4 with a scan rate of 5mV/s and rotation speed of 1,600 r.p.m. **B**) Free energy diagram for oxygen reduction reaction on the g-P-N1-Pt1 catalyst in acidic medium. Adapted with permission from ref. 194. Copyright 2017 Nature Publishing Group.

3.3. Shape Effect:

The facet-controlled synthesis of metal nanocrystals has received extensive attention due to its significant role in tuning the catalytic performance of the nanocrystals.[197-201] As discussed in the previous section of this review, the ORR activity varies at different sites on the surface atom arrangement of crystal planes. Therefore, the shape-controlled synthesis strategy is a promising route to boost Pt activity towards ORR. El-Sayad and coworkers[202-204] have given the

breakthrough by synthesizing a series of shape-controlled colloidal platinum nanoparticles in the shapes of tetrahedral, cubic, irregular-prismatic, icosahedral and cuboctahedral structures. Later on, extensive studies have been performed for the synthesis of shape-controlled well-defined platinum nanocatalysts. Sun and co-workers[205] have developed a very facile shape-controlled synthesis technique for platinum nanoparticles and they established a major effect on the ORR of the PEM fuel cell. They reported that the 7 nm (100)-terminated Pt nanocubes are more active than other shaped Pt NPs, where they credited that the shape-dependent ORR activity of Pt nanoparticles was due to the different adsorption tendency of sulphate ions on Pt(111) and (100) facets .Wang et al.[206] reported that a 7 nm platinum nanoparticle consisting of (111) and (200) facets or only (100) facet transfers nearly four-electron (3.6e) during ORR, whereas 3 and 5 nm nanoparticles with majorly (111) facet transfer less electron (0.7). With the aid of nanocluster models of varying shapes determined by the different facets and their relative distributions, considerable insights on the origin of shape dependent catalytic activity have been obtained recently. Our recent study also shows that cuboctahedral NC favours four-electron reduction, whereas octahedral NC favours two-electron reduction.[44] In this study, we demonstrated using DFT that cuboctahedral nanocluster is more reactive towards ORR than that of octahedral nanocluster due to the presence of (100) facet in the cuboctahedral one. The origin of activity difference is evident from the strain effects of different extents on the NCs. The average Pt–Pt bond distances of the facet atoms are 2.66Å for both the cuboctahedral and octahedral NCs. However, the Pt–Pt bond distance of the (100) facet of the cuboctahedral NC is 2.71 Å. Therefore, due to the presence of two different facets in the cuboctahedral structure, the surface is under strain, which in turn improves the catalytic activity. Moreover, it is experimentally validated that the presence of the (100) facets along with the (111) facets (i.e. cuboctahedral,

truncated-octahedral and hexagonal shape) shows superior catalytic activity than the purely (111) and (100) faceted NCs (i.e. octahedral and cubic shapes). Using the scanning electrochemical microscopy, Sa´nchez et al.[207] reported that the hexagonal platinum nanoparticle with (111) and (100) facets exhibits an enhanced ORR activity while comparing with the sphere (no preferential facets), tetrahedral/octahedral with (111) facets and cubic with (100) facets. The differences in the activity observed in these studies has been attributed to the characteristic binding affinity of facets towards anions in the reaction medium. Owing to the high binding affinity of (100) facets towards SO_4^{2-} ions and (111) facets towards ClO^{4-} ions, having exclusively one of these facets causes blocking of the catalyst surface sites leading to diminished ORR activity. Hence a nanoparticle with both the facets benefit from their cumulative effect on binding of ionic species, and hence results in better catalytic activity.

The shape-dependent ORR activity holds similar trend in Pt-based bimetallic catalysts also. Zhang et al.[208] reported that the Pt_3Ni nanoctahedra terminated with (111) facets improves the specific activity of ORR ($2.75mA/cm^2$) by five-fold and mass activity ($1.1mA/\mu g_{Pt}$) by 2.8 times compared to the similar sized Pt_3Ni nanocube terminated with (100) facets. In this context, Wu et al.[209] investigated a series of Pt_3Ni NCs with fraction of exposed (111) and (100) facets and reported that the truncated-octahedral or cuboctahedral NCs with highly exposed (111) facets increase the ORR mass activity by 1.8 times than that of the octahedral NCs.

Apart from the shape-dependent activity of different facet based nanoparticles, the ORR activity varies with the nanoparticles with similar facets but different overall morphology also. Wu et al.[210] reported that the specific capacity of 13 nm icosahedral Pt_3Ni NPs are 50% higher than that of the octahedral Pt_3Ni NPs even though both shapes are bound by (111) facets. The authors predicted that surface strain-induced electronic effect plays an important role in their ORR

enhancement. Using DFT and Molecular Dynamics simulation of icosahedral and octahedral Pt

nanocrystals with a diameter of 10 nm, the authors demonstrated that the surface strain on an

icosahedral nanoparticle is tensile, whereas it is compressive on an octahedral nanoparticle and

thus making surface strain differences of ~3− 4% (Fig. 17A). Thus, the surface strain shifts the

d-band center of surface atoms, which results in the variations of adsorption strength and
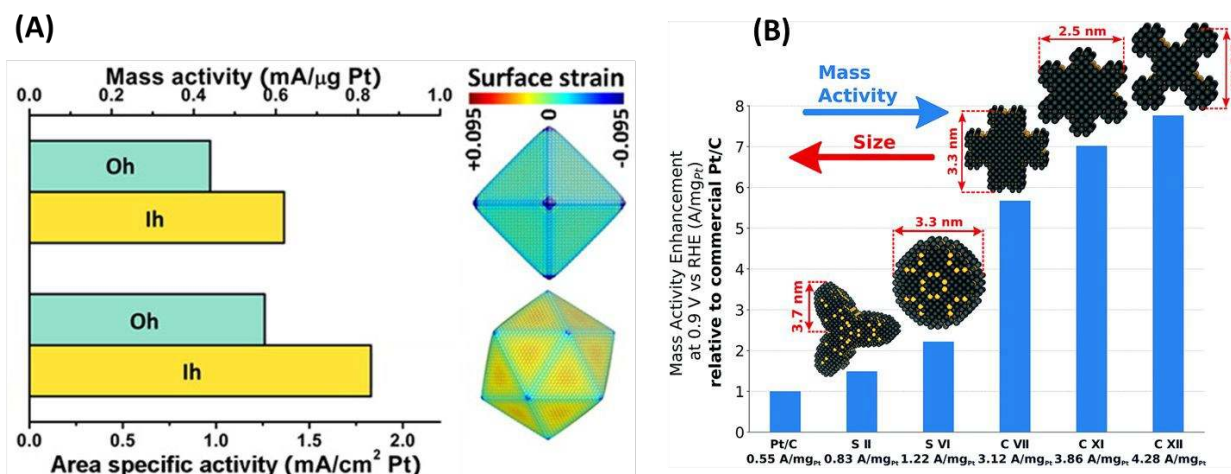
changes the ORR catalytic activity.

Fig. 17(A) Area specific activity and mass activity of icosahedral and octahedral Pt_3Ni and

corresponding surface strain fields. Color is given according to the strain labeled in the color

map. Adapted with permission from ref. 210. Copyright 2012 American Chemical Society, (B)

Mass activities of sphere-like (S II, S VI) and rod-like (C VII, C XI, C XII) nanostructures

obtained from computational screening of nanoparticles over Tanaka commercial Pt/C

electrocatalysts. Adapted with permission from ref. 211. Copyright 2019 Royal Society of

Chemistry.

In this context, a computational screening by Rück et al. reports that the proper tailoring of the

shape of the Pt nanoparticles can boost the mass activities up to 4.28 A/mg$_{Pt}$.[211] Using a fast and

accurate model based on the generalization of Gielis' Superformula[212] for structure designing

followed by optimization toward highest mass activity by the particle swarm optimizer PARPSO[213], they have comprehensively screened over thousands of nanostructures with different shapes and concluded that sphere-like nanoparticles predicts mass activities up to 1.22 A/mg whereas, rod-like nanostructures predict mass activities up to 4.28 A/mg_{Pt}, which is a 7.8-fold enhancement over Tanaka commercial Pt/C electrocatalysts (Fig.17B). Authors have credited the presence of numerous active sites located at concave kinks for such high activities. Furthermore, the proposed nanostructures have been found mechanically as stable as commercial Pt/C electrocatalysts.

3.4. Size Effect:

Size of the nanoparticles plays a significant role towards catalyzing the reaction.[214-216] Smaller nanoparticles are associated with higher surface-to-volume ratios and possess higher amount low-coordinated sites like edges, corners, vertex etc. However, there is a critical particle size, below which catalytic activity can decrease due to less availability of active reaction sites. Besides, the metal-to-insulator transition and Coulomb blockade effect appear which can also lower the electrochemical activity[217,218]. For theoretical studies as well, the size reduction beyond a limit is not preferred, as the system no longer exhibits the properties of metal but behave as molecular clusters. Similarly, the nanoparticles behaves like bulk (although reaction and metal specific) after sizes greater than 5nm. The optimum size of the nanocluster considered for theoretical modelling is a matter of both experimentally important parameters such as shape, geometry etc. as well as that of computational expenditure. Tritsaris et al. made an observation that the activity of nanoclusters achieves a saturation point with highest mass activity predicted for nanoparticles of diameters 2-4 nm.[219] They have also observed that the low coordinated atoms do not affect the activities of other sites as their number decreases with increment in the

size of the nanoparticle. Hence a size close to ~2-4 nm where we can have analogous properties of even bigger size NCs such as relative ratio of different facets, facet vs edge sites as well as enough adsorption sites to have a coverage study can be considered as an optimum size of the nanoclusters for theoretical modelling.

Based on the ORR activity vs. size of the Pd@Pt core nanocluster, Adzic and coworkers[220] reported that particle size of the nanocluster affects the fraction of active sites at surface as well as the turnover frequency (TOF) per active site. The product of the two effects eventually determines the specific activity of the catalysts. They reported that the optimal binding energy of O-atom (lower by 0.2 eV from Pt (111) surface) can be achieved on Pt nanoparticle with the size of 1.8 nm where the nanosize-induced surface contraction plays the crucial role. On the other hand, the optimal *O binding energy is found using the 3.4 and 4.4 nm sized core-shell (Pd@Pt) nanoparticles where the reduced nanosize effect is compensated by increased influence of Pd core.

An et al.[221] computationally reported the size and shape effects of a Pd core with Pt shell (Pd@Pt) nanoparticles with size from 1 to 3 nm (35−405 atoms) with shapes of tetrahedron (TH) and sphere-like truncated octahedron (SP) as has been shown in Fig. 18A. They demonstrated that with the increasing of particle size the stability of the nanoclusters increases showing bulk like behavior after certain size. It has been that credited that the stability is associated with the surface contraction (Fig. 18B & C). The surface contraction, which arises due to the atomic size mismatch of the atoms (between Pd and Pt atoms) and finite size effects, decreases with the increases of particle size. A significant surface contraction exists for particle size less than 3 and likely even 4 nm. Interestingly, a volcano-like relationship between the *O binding energy and particle size is observed for the SP NPs, whereas an exponential decay of binding energy is

obtained in the case of TH NPs (Fig. 18D). Authors claimed that interplay between surface contraction and local structural flexibility of the nanoparticle occurs. The SP nanoclusters with the size of 2.2-5 nm bind O-atom moderately to catalyze the ORR efficiently without compromising the stability issue during the reaction (Fig. 18E).

Chorkendorff and coworkers investigated the effect of size upon the ORR activity of Pt particles with diameters ranging from 2 to around 11 nm and reported the highest mass activity($1A/mg_{Pt}$) for 3nm sized nanoparticles.[222] Leontyev et al.[223] studied the size-dependent catalytic activity of carbon-supported Pt catalysts in the size range of 1.8-5.4 nm and reported that decreasing particle size improves catalytic activity upto the average size of 2.7 nm with highest mass activity due to the very high fraction of (111) facet. Shao et al.[224] reported that both mass activity and specific activity for ORR are low for particle sizes of platinum smaller than 2.2 nm (0.1 A/mg_{Pt} and 0.12 mA/cm^2) and they mentioned that strong O-binding sites (edge sites) increases in nanoparticles smaller than 2.2 nm. In contrast, Nesselberger et al.[225] reported that the mass activity increased linearly with increasing catalyst dispersion regardless, whereas the specific activity does not changes significantly between the nanoparticle sizes of 1-5 nm. They commented that the reaction pathway of the ORR changes with the particle size. The strong binding energy of O-atom on smaller Pt-particles influence the reaction pathway to proceed through direct O-O direction instead of undergoing proton and electron transfer to oxygen molecule.
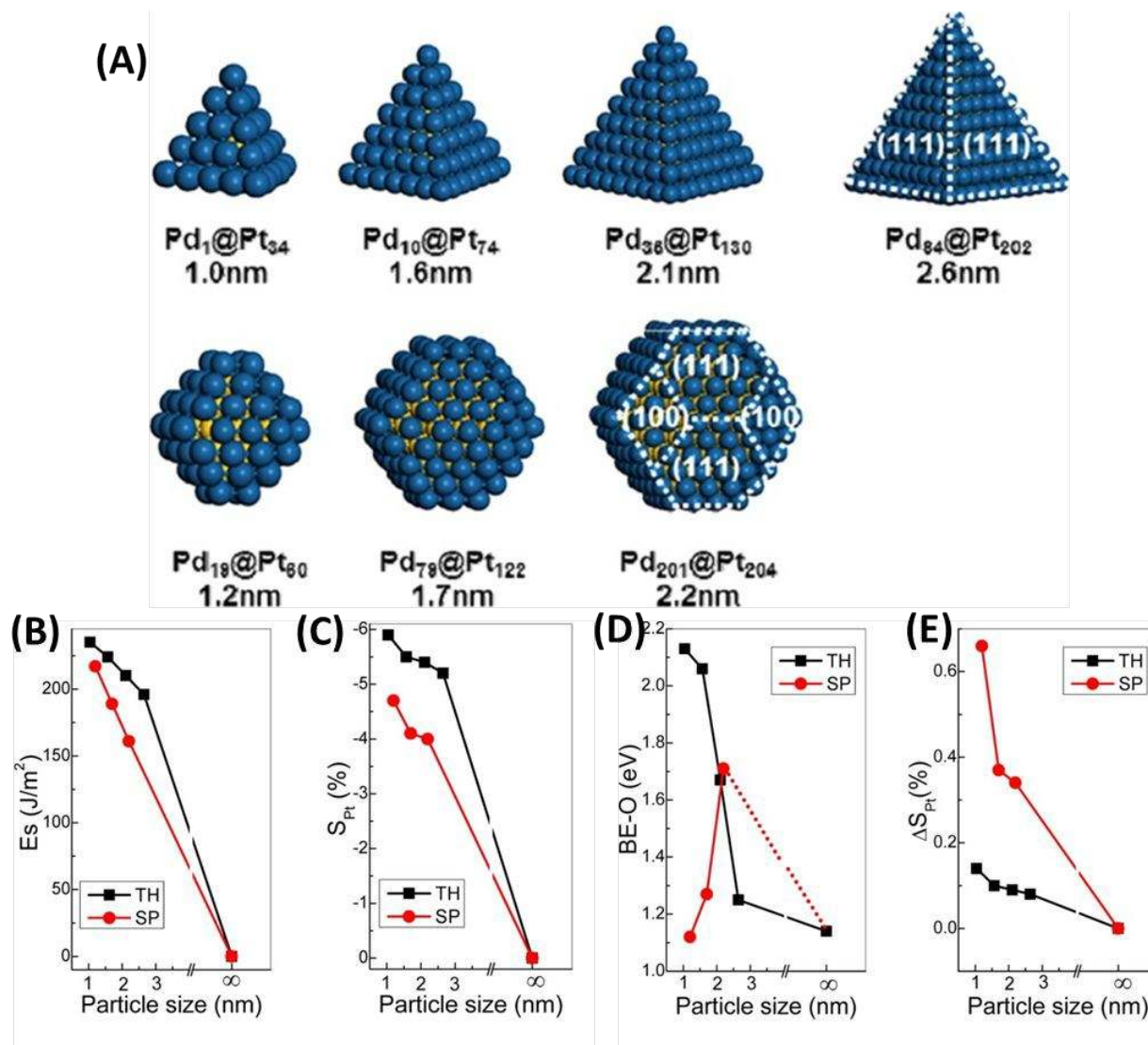
Fig. 18: (A) Pd@Pt core−shell NPs in different sizes and shapes (blue, Pt; yellow, Pd). Top: TH. Bottom: SP. (B) Relative stability and (C) Relative surface contraction of Pd@Pt core−shell NPs with respect to Pt/Pd(111) as a function of particle size. (D) O-binding energy at 3-fold hollow sites on the (111) terrace of TH and SP NPs as a function of particle size. (E) Relative variation with respect to Pt/Pd(111) in (111) surface contraction before and after O adsorption as a function of particle size. Adapted with permission from ref. 221. Copyright 2013, American Chemical Society.

In this context, apart from *O binding energy, Rück et al.[87] demonstrated that there is a linear scaling relation between *OH adsorption energies and generalized coordination numbers for multifaceted Pt nanoparticles irrespective of the shapes (such as tetrahedrons, cuboctahedrons, truncated octahedrons, and extended surfaces) and further using a computationally inexpensive nanoparticles screening model, concluded that the highest mass activity can be obtained at nanoparticle diameters of 1, 2, and 2.9 nm for nanoparticle size distributions below 0.2 nm (Fig. 19). The mass activity vs. particle size trend shown by Rück et al. nicely matches with the experimental work by Perez-Alonso et al.[222] and Shao et al.[224] Later on, a joint computational and experimental work by Garlyyev et al.[226] synthesized a 1 nm sized Pt NP anchored with MOF with the highest mass activity of 0.87 ± 0.14 AmgPt^{-1} among pure Pt-based electrocatalysts of similar sizes. More importantly, the mass activity value nicely matches with the computational prediction of 0.99 Amg/Pt, using the model developed by Ruck et al. for the 1.1 nm NP with size distribution of 0.17 nm.
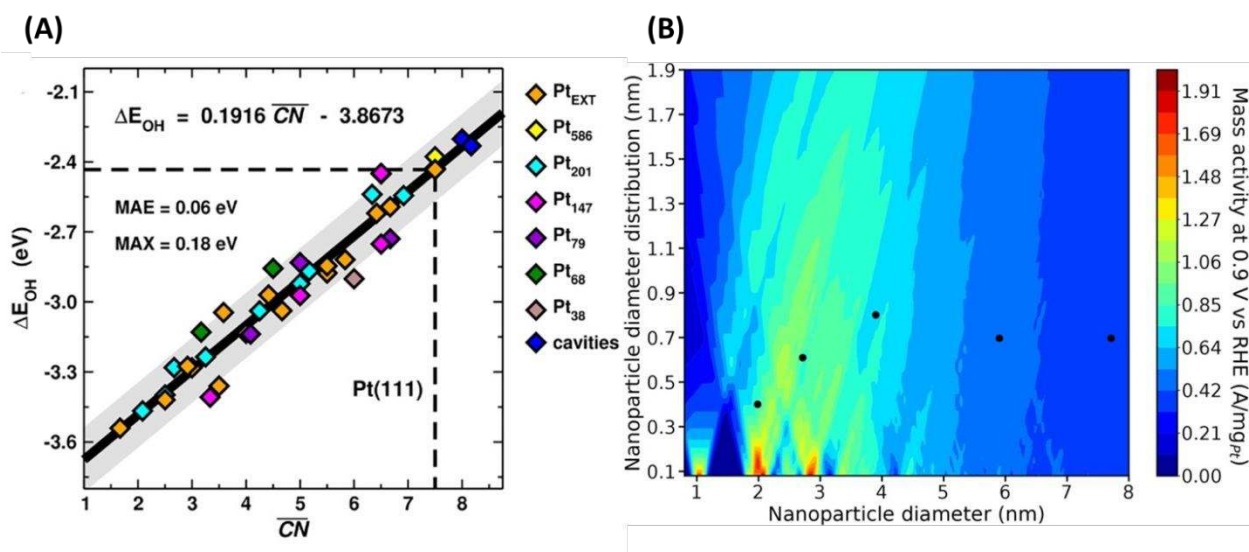
Fig. 19: (A) DFT calculated *OH adsorption energies (ΔE_{OH}) are on diversely coordinated sites in different catalyst shapes with varying sizes; such as tetrahedrons (green),cuboctahedrons (magenta), truncated octahedrons (yellow, cyan, purple, brown), extended surfaces (orange), and cavities (blue). The linear dependence between ΔE_{OH} and the generalized coordination number (CN) is described by the linear function provided in the inset. The ±2MAE around the linear fit is indicated by the gray area containing 75% of the calculated data points. (B) Contour plot depicting the full parameter space of the particle size effect. Nanoparticle diameters and associated diameter distributions on the horizontal axis and the vertical axis, respectively are mapped onto the catalytic activity indicated by the color plot. Black dots represent experimental data obtained from reference 222. The contour plot reveals that highest mass activities (indicated by red colored areas) are offered by nanoparticles at diameters of 1, 2, and 2.9 nm with diameter distributions below 0.2 nm. Adapted with permission from ref. 87. Copyright 2018 American Chemical Society

3.5 Some other determining factors

In addition with the shape and size effects, some other parameters have been recently put forwarded from theoretical studies with potential to address some of the challenges associated with oxygen reduction reaction and paved way towards controlling the catalytic activity in desirable manner. For example, Bhattacharjee and Lee[227] have proposed that the binding of ORR intermediates on a structurally ordered PdFe surface can be controlled via relative spin orientations between intermediates and the surface. They have observed a weakening of binding strength of ORR intermediates and a high rate for O_2 dissociation on the ferromagnetic surface through constrained DFT calculations. The authors propose that this can be achieved in an experimental scenario by applying an optimum magnetic field, which can control the spin

orientations of adsorbate species. Although this work does not consider platinum as a constituent metal, the plausibility of spin control over catalytic activity can be expected to provide new platforms for alloys of Pt transition metals having magnetic nature. Another area of immense research interest is designing new catalyst supporting materials ranging from conventional 2D materials like graphene, doped nanosheets, single or multiwalled carbon nanotubes and so on.[228-230] These materials are extensively investigated for their capability to act as strong supports for anchoring the nanocatalysts as well their interaction with the catalysts resulting in the modification of electronic structure of catalysts hence improving the ORR activity.

4. Conclusions and Outlook

Significant progress in PEM fuel cell catalysis has been made in the last two decades for the commercialization of fuel cell industry. State-of-the-art catalysts for fuel cell applications are still restricted to Pt-based, mainly carbon-supported Pt catalysts. In this review, the breakthrough achievements towards addressing the major challenges such as high Pt-loadings, low ORR activities and low stability have been reviewed with a detailed investigation of the theoretical understanding for overcoming these challenges. The achievements on Pt-nanostructured catalysts are mainly directed towards: i) high-index based Pt-surface, ii) Pt-alloy like core-shell, Pt-skin based catalysts, and iii) hollow, sheet and wire kind of nanostructures. The important remarks and future directions the review suggests for the empowerment of fuel cell catalysis research are discussed below:

- The recent decades have witnessed compelling research ventures to achieve the expected fuel cell efficiency by designing efficient nanostructure based catalysts for oxygen reduction reaction. By the effective tuning of structure, composition, shape and size

factors of nanostructures of different dimensions, further significant improvements can be achieved in this regime

- Nanocluster modelling studies are extremely helpful in understanding the structure, shape and size dependent activity of nanoparticles. They provide a sound platform to explore the possibility of desirable tuning of key ORR parameters such as adsorption energetics, overpotential, activation barrier and so on which can have a direct manifestation in the experimental scenario.

- High-index nanostructures have shown promising ORR performance but less explored and this area should be an on-going research topic towards novel catalyst development. As high-index nanocluster contains several types of adsorption sites and hence a conjoint theoretical and experimental analysis on high-index based nanocluster can provide remarkable information regarding the reaction energetics at at different sites which eventually helps to design high-index based catalysts with desired geometry.

- The enhancement of catalyst activity and stability on Pt-alloys and core shell particles is strongly dependent on geometric and electronic effects generated by the non-Pt metal of the alloy, while the composition is very important in modifying the surface structure of Pt-alloys. Based on authors viewpoint, the adsorbate-induced surface modification is a big scope to look into along with the ligand and strain effect where computational screening studies can have a decisive role in reducing the trial and error efforts of experimentalists by providing useful thumbnails on potential candidate compositions for ORR.

- Recent success on thin nanostructures (cage, sheet and wires) shows their potential as promising ORR catalysts. Due to presence of low-coordinated adsorption sites, the

reaction intermediates might prefer to bind on some different sites with that on Pt (111) surface, which eventually can affect the reaction mechanism. Therefore, the identification of active sites on these nanostructures is very crucial and is an important area where theoretical studies on modelled structures can help to elucidate it.

- Factors like size, shape and morphology of the catalyst are decisive in changing the number of active sites on the catalyst surface as well as stabilizing the surface structure. By wisely conjoining the theoretical understanding of activity dependence on these factors with sophisticated experimental techniques, enhanced ORR activity can be expected.

- Non-conventional approaches such as single atom catalysts for minimum platinum loading, magnetic effects for controlling regulating the behavior of adsorbates on the catalyst surface and so on can be explored and can be influential in driving the development of novel catalyst materials.

- Developing efficient catalysts for oxygen reduction in fuel cells is an area of utmost research interest where highly subtle concerted studies from theoretical and experimental perspectives are being performed. By further successful combination of theoretical strategies with synthetic principles, ideal efficiency of a fuel cell can be expected to be attained within the immediate future

Conflicts of Interest

The authors declare no conflicts of interest.

References:

1. F. A. de Bruijn, V. A. T. Dam and G. J. M. Janssen, *Fuel Cells*, 2008, **8**, 3-22.

2. C. Qin, J. Wang, D. Yang, B. Li and C. Zhang, *Catalysts*, 2016, **6**, 197.

3. J. Wu and H. Yang, *Acc. Chem. Res*., 2013, **46**, 1848-1857.

4. M. Watanabe, D. A. Tryk, M. Wakisaka, H. Yano and H. Uchida, *Electrochimica Acta*. 2012, **84**, 187-201.

5. O. T. Holton and J. W. Stevenson, *Platinum Metals Rev*. 2013, **57**, 259-271.

6. S. Sui, X. Wang, X. Zhou, Y. Su, S. Riffat and C. Liu, *J. Mater. Chem. A.*, 2017, **5**, 1808-1825.

7. P. B. Balbuena, R. Callejas-Tovar, P. Hirunsit, J. M. Martı´nez de la Hoz, Y. Ma and G. E. Ramı´rez-Caballero, *Top Catal*., 2012. **55**, 322-335.

8. F. T. Wagner, B. Lakshmanan and M. F. Mathias, *J. Phys. Chem. Lett*., 2010, **1**, 2204-2219.

9. M. K. Debe, *Nature*, 2012, **486**, 43.

10. A. Kongkanand and M. F. Mathias, *J. Phys. Chem. Lett*., 2016, **7**, 1127−1137.

11. E. Proietti, F. Jaouen, M. Lefèvre, N. Larouche, J. Tian, J. Herranz and J.-P. Dodelet, *Nat. Comm*., 2011, **2**, 416.

12. W. Xiao, M. A. L. Cordeiro, M. Gong, L. Han, J. Wang, C. Bian, J. Zhu, H. L. Xin, and D. Wang, *J. Mater. Chem. A*, 2017, **5**, 9867-9872.

13. R. K. Gupta, A. D. Verma, I. Sinha and M. Malviya, *Chem. Phy. Lett.*, 2017, **680**, 6-9.

14. Z. Jin, P. Li and D. Xiao, *Scientific Reports*, 2014, **4**, 6712.

15. D. H. Youn, G. Bae, S. Han, J. Y. Kim, J. W. Jang, H. Park, S. H. Choic and J. S. A. Lee, *J. Mater. Chem. A*, 2013, **1**, 8007-8015.

16. B. Cao, J. C. Neuefeind, R. R. Adzic and P. G. Khalifah, *Inorg. Chem.*, 2015, **54**, 2128-2136.

17. S. J. Rowley-Neale, J. M. Fearn, D. A. C. Brownson, G. C. Smith, X. Jic and C. E. Banks, *Nanoscale*, 2016, **8**, 14767-14777.

18. H. Wang, Y. Liang, Y. Li and H. Dai, *Angew. Chem.*, 2011, **123**, 11161-11164.

19. Z. Chen, D. Higgins, H. Tao, R. S. Hsu and Z. Chen, *J. Phys. Chem. C*, 2009, **113**, 21008-21013.

20. M. del Cueto, P. Ocón and J. M. L. Poyato, *J. Phys. Chem. C*, 2015, **119**, 2004–2009.

21. D. Yu, Q. Zhang and L. Dai, *J. Am. Chem. Soc.*, 2010, **132**, 15127-15129.

22. C. R. Raj, A Samanta, S. H. Noh, S. Mondal, T. Okajima and T. Ohsaka, *J. Mater. Chem. A*, 2016, **4**, 11156-11178.

23. K. E. Swider-Lyons and S. A. Campbell, *J. Phys. Chem. Lett.*, 2013, **4**, 393-401.

24. X. Wang, S. Choi, L. T. Roling, M. Luo, C. Ma, L. Zhang, M. Chi, J. Liu, Z. Xie, J. A. Herron, M. Mavrikakis and Y. Xia, *Nat. Chem.*, 2005, **6**, 7594.

25. O. Oezaslan, F. Hasche and P. Strasser *J. Phys. Chem. Lett.*, 2013, **4**, 3273-3291.

26.   V. Mazumder, M. Chi, K. L. More, S. Sun, *J. Am. Chen. SOC.*, 2010, **132**, 7848-7849.

27.   S. Fu, C. Zhu, J. Song, M. H. Engelhard, H. Xia, D. Du and Y. Lin, *ACS Appl. Mater. Interfaces*, 2016, **8**, 35213-35218.

28.   G. Zhang, S. Sun, M. C. Y. Zhang, R. Li and X. Sun, *Scientific reports*, 2013, **3**, 1526.

29.   D. S. He, D. He, J. Wang, Y. Lin, P. Yin, X. Hong, Y. Wu and Y. Li, *J. Am. Chem. Soc.*, 2016, **138**, 1494-1497.

30.   H. Liu, P. Zhong, K. Liu, L. Han, H. Zheng, Y. Yin and C. Gao, *Chem. Sci.*, 2018, **9**, 398–404.

31.   A. Mahata, P. Garg, K. S. Rawat, P. Bhauriyal and B. Pathak, *J. Mater. Chem. A*, 2017, **5**, 5303-5313.

32.   M. Shao, Q. Chang, J. Dodelet and R. Chenitz, *Chem. Rev.*, 2016, **116**, 3594-3657.

33.   Y. Nie, L. Li and Z. Wei, *Chem. Soc. Rev.*, 2015, **44**, 2168-2201.

34.   J. K. Nørskov, J. Rossmeisl, A. Logadottir and L. Lindqvist, *J. Phys. Chem. B*, 2004, **108**, 17886-17892.

35.   Y. Sha, T. H. Yu, Y. Liu, B. V. Merinov and W. A. Goddard, *J. Phys. Chem. Lett.*, 2010, **1**, 856-861.

36.   T. Zhang and A. B. Anderson, *Electrochim. Acta.* 2007, **53**, 982-989.

37.   Y. Jiao, Y. Zheng, Y. Jaroniec and S. Z. Qiao, *Chem. Soc. Rev.,* 2015, **44**, 2060-2086.

38.   J. A. Keith, G. Jerkiewicz and T. Jacob, *ChemPhysChem.*, 2010, **11**, 2779-2794.

39. A. Kulkarni, S. Siahrostami, A. Patel and J. K. Nørskov, *Chem. Rev.,* 2018, **118**, 2302-2312.

40. V. Tripkovi´ca, E. Skúlasona, S. Siahrostamia, J. K. Nørskov and J. Rossmeisl, *Electrochimica Acta*, 2010, **55**, 7975-7981.

41. H. A. Hansen, V. Viswanathan and J. K. Nørskov, *J. Phys. Chem. C*, 2014, **118**, 6706-6718.

42. A. Zadick, L. Dubau, N. Sergent, G. Berthome and M. Chatenet, *ACS Catal.*, 2015, **5**, 4819-4824.

43. Z. Zhang, J. Liu, J. Gu, L. Sub and L. Cheng, *Energy Environ. Sci.*, 2014, **7**, 2535-2558.

44. A. Mahata, K. S. Rawat, I. Choudhuri, and B. Pathak, *Catal. Sci. Technol.*, 2016, **6**, 7913-7923.

45. A. Mahata, P. Bhauriyal, K. S. Rawat and B. Pathak, *ACS Energy Lett.*, 2016, **1**, 797-805.

46. M. P. Hyman and J. W. Medlin, *J. Phys. Chem. B,* 2006, **110**, 15338-15344.

47. N. G. Araez, *J. Phys. Chem. C*, 2011, **115**, 501-510.

48. X. Ge, A. Sumboja, D. Wuu, T. An, B. Li, F. W. Goh, T. S. H. Hor, Y. Zong and Z. Liu, *ACS Catal.*, 2015, **5**, 4643-4667.

49. O. Antoine, Y. Bultel and R. Durand, *J. Electroanal. Chem.*, 2001, **499**, 85-94.

50. S. B. Sepa, M. V. Voinovic and A. Damjanovic, *Electrochim. Acta.*, 1981, **26**, 781-793.

51. A. Damjanovic and V. Brusic, *Electrochim. Acta*. 1967, **12**, 615–628.

52.	Q. Jia, K. Caldwell, J. M. Ziegelbauer, A. Kongkanand, F. T. Wagner, S. Mukerjee, and D. E. Ramakerb, *J. Electrochem. Soc*., 2014, **161**, F1323-F1329.

53.	V. Stamenkovic´, T.J. Schmidt, P. N. Ross and N. M. Markovic, *J. Phys. Chem. B*, 2002, **106**, 11970-11979.

54.	J. Greeley and M. Mavrikakis, *Nat. Mater*. 2004, **3**, 810–815.

55.	L. Ou and S. Chen, *J. Phys. Chem. C*. 2013, **117**, 1342-1349.

56.	K. Li, Y. Li, Y. Wang, F. He, M. Jiao, H. Tang and Z. Wu, *J. Mater. Chem. A*, 2015, **3**, 11444-11452.

57.	Z. Duan and G. Wang, *Phys. Chem. Chem. Phys*. 2011, **13**, 20178-20187.

58.	Y. Sha, T. H. Yu, B. V. Merinov, P. Shirvanian and W. A. Goddard, *J. Phys. Chem. Lett*., 2011, **2**, 572–576.

59.	R. F. de Morais, A. A. Franco, P. Sauteta and D. Loffreda, *Phys. Chem. Chem. Phys*. 2015, **17**, 11392-11400.

60.	L. Qi, J. Yu and J. Lia, *J. Chem. Phys*., 2006, **125**, 054701.

61.	P. D. Nolan, B. R. Lutz, P. L. Tanaka, J. E. Davis and C. B. Mullinsa, J. *Chem. Phys*., 1999, **111**, 3696.

62.	M. J. Janik, C. D. Taylor and M. Neurockc, *J. Electrochem. Soc*., 2009, **156**, B126.

63.	K. Yeh and M. J. Janik, *J. Comput. Chem*., 2011, **32**, 3399.

64.	S. A. Wasileski and M. J. Janik, *Phys. Chem. Chem. Phys*., 2008, **10**, 3613.

65.	S. Sakong, M. Naderian, K. Mathew, R. G. Hennig and A. Groß, *J. Chem. Phys*., 2015, **142**, 234107.

66.	S. Sakong and A. Groß, *ACS Catalysis*., 2016, **6**, 5575-5586.

67.	J. Carrasco, A. Hodgson and A . Michaelides, *Nat. Mater*., 2012, **11**, 667-674.

68.   S. Schnur and A. Groß, *New J. Phys*., 2009, **11**, 125003.

69.   M. Garcia-Ratés, R. García-Muelas and N. López, *J. Phys.Chem*., 2017, **121**, 13803-13809.

70.   Q. Zhang and A. Asthagiri, *Catalysis Today*., 2019, **323**, 35-43.

71.   F. Calle-Vallejo, R. F. de Morais, F. Illas, D. Loffred and P. Sautet, *J. Phys. Chem. C.*, 2019, **123,** 95578-5582.

72.   P. W. Atkins, Physical Chemistry, Oxford University Press, Oxford,1990.

73.   G. Ertl, *Surf. Sci*., 1994, **299**, 742.

74.   R. J. Baxter and P. Hu, *J. Chem. Phys*., **116**, 2002, 4379.

75.   G. S. Karlberg, J. Rossmeisl and J. K. Nørskov, *Phys. Chem. Chem. Phys*., 2007, **9**, 5158-5161.

76.   M. T. M. Koper, *J. Electroanal. Chem.* 2011, **660**, 254-260.

77.   M. G. Evans and M. Polanyi, *Trans. Faraday Soc.* 1938*,* **34**, 11-24.

78.   A. Michaelides, Z. P. Liu, C. J. Zhang, A. Alavi, D. A. King and P. Hu, *J. Am. Chem. Soc*., 2003, **125**, 3704-3705.

79.   V. Viswanathan, H. A. Hansen, J. Rossmeisl and J. K. Nørskov, *ACS Catal*., 2012**, 2**, 1654-1660.

80.   H.- Y. Su, K. Sun, W.-Q. Wang, Z. Zeng, F. Calle-Vallejo and W.-X. Li, *J. Phys. Chem. Lett*., 2016, **7**, 5302-5306.

81.   F. Calle-Vallejo, A. Krabbeb and J. M. Garc´ıa-Lastra, *Chem. Sci*., 2017, **8**, 124-130.

82.   N. Govindarajan, J. M. García-Lastra, E. J. Meijer and F.Calle-Vallejo. *Curr. Opin. Electrochem*., 2018, **8**,110–117.

83. F. Calle-Vallejo, D. Loffreda, M. T. M. Koper and P. Sautet, *Nat. Chem.*, 2015, **7**, 403–410.

84. F. Calle-Vallejo, J. I. Martnez, J. M. Garcia-Lastra, P. Sautet and D. Loffreda, *Angew. Chem. Int. Ed.* 2014, **53**, 1 – 5.

85. F. Calle-Vallejo, M. D. Pohl, D. Reinisch, D. Loffreda, P. Sautet and A. S. Bandarenka, *Chem. Sci.,* 2017, **8**, 2283–2289.

86. J. L. Lansford. A. V. Mironenko and D. G. Vlachos, *Nat. Comm,* 2017, **8**, 1842.

87. M. Ruck, A. Bandarenka, F. Calle-Vallejo and A. Gagliardi, *J. Phys. Chem. Lett.*, 2018, **9**, 4463−4468.

88. S. Mostafa, F. Behafarid, J. R. Croy, L. K. Ono, L. Li, J. C. Yang, A. I. Frenkel and B. R. Cuenya, *J. Am. Chem. Soc.*, 2010, **132**, 15714–15719.

89. B. R. Cuenya, *Acc. Chem. Res.*, 2013, **46**, 1682-1691.

90. V. Komanicky, H. Iddir, K.-C. Chang, A. Menzel, G. Karapetrov, D. Hennessy, P. Zapol and H. You, *J. Am. Chem. Soc.*, 2009, **131**, 5732-5733.

91. C. Y. Chiu, Y. Li, L. Ruan, Y. Ye, C. B. Murray and Y. Huang, *Nat. Chem.*, 2011, **3**, 393-399.

92. V. L. Nguyen, M. Ohtaki, V. N. Ngo, M. T. Cao and M. Nogami, *Adv. Nat. Sci. Nanosci. Nanotechnol.*, **2012**, 3, 025005.

93. Y. Xia, Y. Xiong, B. Lim and S. E. Skrabalak, *Angew. Chem. Int. Ed.*, 2009, **48**, 60-103.

94. R. Zheng, H. Gu, B. Xu, K. K. Fung, X. Zhang and S. P. Ringer, *Adv. Mater.*, 2006, **18**, 2418-2421.

Catalysis Science & Technology Accepted Manuscript

95. N. M. Markovic, H. Gasteiger and P. N. Ross, *J. Electrochem. Soc*., 1997, **144**, 1591-1597.

96. K. Kinoshita. *J. Electrochem. Soc*., 1990, **137**, 845-848.

97. J. M. Feliu, A. Fernandez-Vega, A. Aldaz and J. Clavilier, *J. Electroanal. Chem. Interfacial. Electrochem.,* 1988, **256**, 149-163.

98. Z.-Y. Zhou, Z.-Z. Huang, D.-J. Chen, Q. Wang, N. Tian and S.-J. Sun, *Angew. Chem. Int. Ed*., 2010, **49**, 411–414.

99. N. Tian, Z. Y. Zhou and S. G. Sun, *J. Phys.* Chem. *C*, 2008, **112**, 19801–19817.

100. Y.-J. Wang, W. Long, L. Wang, R. Yuan, A. Ignaszak, B. Fang and D. P. Wilkinson, *Energy Environ. Sci*., 2018, **11**, 258-275.

101. N. Tian, Z. Y. Zhou, S. G. Sun, Y. Ding and Z. L. Wang, *Science.* 2007, **316**, 732-735.

102. T. Yu, D. Y. Kim, H. Zhang and Y. Xia, *Angew. Chem. Int. Ed*., 2011, **50**, 2773 – 2777.

103. B. Y. Xia, H. B. Wu, X. Wang and X. W. Lou, *Angew. Chem. Int. Ed*., 2013, **52**, 12337 -12340.

104. M. D. Macia, J. M. Campina, E. Herrero and J. M. Feliu, *J. Electroanal. Chem*., 2004, **564**, 141–150.

105. A. Kuzume, E. Herrero and J. M. Feliu, *J. Electroanal. Chem*., 2007, **599**, 333-343.

106. R. Rizo, E. Herrero and J. M. Feliu, *Phys. Chem. Chem. Phys.,* 2013, **15**, 15416-15425.

107. N. Hoshi, M. Nakamura and A. Hitotsuyanagi, *Electrochimica Acta*., 2013, **112**, 899-904.

108. B. B. Xiao, X. B. Jiangb and Q. Jiang, *Phys. Chem. Chem. Phys.,* 2016, **18**, 14234-14243.

109. S. Kattel, Z. Duan and Z. Wang, *J. Phys. Chem. C*, 2013, **117**, 7107-7113.

110. H.-T. Tsai, Y.-C. Hsieh, T. H, Yu, Y.-J. Lee, Y.-H. Wu, B. V. Merinov, P.-W. Wu, S.-Y. Chen, R. R. Adzic and W. A. Goddard, *ACS Catal.*, 2015, **5**, 1568-1580.

111. J. Greely, J. Rossmeisl, A. Hellman and J. K. Nørskov, *J. Phys. Chem. C*, 2007, **221**, 1209-1220.

112. G. A. Tritsaris, J. Greely and J. K. Nørskov. *Catal. Lett.*, 2011, **141**, 909-913.

113. A. Hitotsuyanagi, S. Kondo, M. Nakamura and N. Hoshi, *J. Electroanal. Chem.*, 2011, **657**, 123-127.

114. A. Hitotsuyanagi, M. Nakamura and N. Hoshi, *Electrochim. Acta.* 2012, **82**, 512-516.

115. A. S. Bandarenka, H. A. Hansen, J. Rossmeisl and I. E. L. Stephens, *Phys. Chem. Chem. Phys.*, 2014, **16**, 13625-13629.

116. A. Nagoya, R. Jinnouchi, K. Kodama and Y. Morimoto, *J. Electroanal. Chem.* 2015, **757**, 116-127.

117. R. Jinnouchi, K. Kodama, A. Nagoya and Y. Morimoto, *Electrochimica Acta*, 2017, **230**, 470-478.

118. J. Yue, Z. Du and M. Shao, *J. Phys. Chem. Lett.*, 2015, **6**, 3346-3351.

119. G. A. Tritsaris, J. Greeley, J. Rossmeisl and J. K. Nørskov, *Catal Lett.*, 2011, **141**, 909-913.

120. V. Stamenković, T. J. Schmidt, P. N. Ross and N. M. Marković, *J. Phys. Chem. B.* 2002, **106**, 11970-11979.

121. V. R. Stamenkovic, B. S. Mun, M. Arenz, K. J. J. Mayrhofer, C. A. Lucas, G. Wang, P. N. Ross and N. M. Markovic, *Nat. Mater.*, 2007, **6**, 241-247.

122. V. R. Stamenkovic, B. M. Mun, K. J. J. Mayrhofer, P. N. Ross and N. M. Markovic, *J. Am. Chem. Soc.*, 2006, **128**, 8813–8819.

123. J. K. Nørskov, F. Abild-Pedersena, F. Studt and T. Bligaard, *Proc. Natl. Acad. Sci. U.S.A.*, 2011, **108**, 937-943.

124. F. H. B. Lima, J. Zhang, M. H. Shao, K. Sasaki, M. B. Vukmirovic, E. A. Ticianelli, and R. R. Adzic, *J. Phys. Chem. C*, 2007, **111**, 404-410.

125. Z. Duan, J. Zhong and G. Wang, *J. Chem. Phys.*, 2010, **133**, 114701-114710.

126. S. Kattel and G. Wang, *J. Chem. Phys.*, 2014, **141**, 124713-124718.

127. J. R. Kitchin, J. K. Nørskov and M. A. Barteau, J. G. Chen, *J. Chem. Phys.*, 2007, **120**, 10240-10246.

128. T. Hofmann, T. H. Yu, M. Folse, L. Weinhardt, M. Bar, Y. Zhang, B. V. Merinov, D. J. Myers, W. A. Goddard and C. Heske, *J. Phys. Chem. C*, **2012**, 116, 24016–24026.

129. H. Xin and S. Linic, *J. Chem. Phys.*, 2010, **132**, 221101.

130. S. Back and Y. Jung, *ChemCatChem.*, 2017, **9**, 3173–3179.

131. V. R. Stamenkovic, B. Fowler, B. S. Mun, G. Wang, P. N. Ross, C. A. Lucas, and N. M. Markovic, *Science*, 2007, **315**, 493-496.

132. V. R. Stamenkovic, B. S. Mun, M. Arenz, K. J. J. Mayrhofer, C. A. Lucas, G. Wang, P. N. Ross and N. M. Markovic, *Nat. Mater.*, 2007, **6**, 241-247.

133. C. Wang, G. Wang, D. van der Vliet, K. C. Chang, N. M. Markovic and V. R. Stamenkovic, *Phys. Chem. Chem. Phys.*, 2010, **12**, 6933–6939.

Catalysis Science & Technology Accepted Manuscript

134. C. Wang, D. van der Vliet, K.-C. Chang, H. You, D. Strmcnik, J. A. Schlueter, N. M. Markovic and V. R. Stamenkovic, *J. Phys. Chem. C*, 2009, **113**, 19365–19368.

135. D. van der Vliet, C. Wang, D. Li, A. P. Paulikas, J. Greeley, R. B. Rankin, D. Strmcnik, D. Tripkovic, N. M. Markovic and V. R. Stamenkovic, *Angew. Chem.*, 2012, **124**, 3193–3196.

136. J. Greeley, I. E. L. Stephens, A. S. Bondarenko, T. P. Johansson, H. A. Hansen, T. F. Jaramillo, J. Rossmeisl, I. Chorkendorff and J. K. Nørskov, *Nat. Chem.*, 2009, **1**, 552-556.

137. M. A. Escribano, P. Malacrid, M. H. Hansen, U. G. Vej-Hansen, A. P. Palenzuela, V. Tripkovic, J. Schiøtz, J. Rossmeisl, I. E. L. Stephens and I. Chorkendorff1, *Science.* 2016, **352**, 73-76.

138. C. Wang, D. Li, M. Chi, J. Pearson, R. B. Rankin, J. Greeley, Z. Duan, G. Wang, D. van der Vliet, K. L. More, N. M. Markovic and V. R Stamenkovic, *J. Phys. Chem. Lett.*, 2012, **3**, 1668-1673.

139. S. Fu, C. Zhu, D. Du and Y. Lin, *ACS Appl. Mater. Interfaces.*, 2016, **8**, 6110−6116.

140. Y. Bing, H. Liu, L. Zhang, D. Ghosh and J. Zhang, *Chem. Soc. Rev.*, 2010, **39**, 2184-2202.

141. H. R. Colon-Mercado and B. N. Popov, *J. Power Sources*, 2006, **155**, 253-263.

142. S. Mezzavilla, C. Baldizzone, A.–C. Swertz, N. Hodnik, P. Pizzutilo, G. Polymeros, G. P. Keeley, J. Knossalla, M. Heggen, K. J. J. Mayrhofer and F. Schüth, *ACS Catal.*, 2016, **6**, 8058-8068.

143. H.-T. Sai, T. H. Yu, Y. Sha, B. V. Merinov, P.-W. Wu, S.-Y. Chen and W. A. Goddard III, *J. Phys. Chem. C*, 2014, **118**, 26703-26712.

144. A. U. Nilekar and M. Mavrikakis, *Surf. Sci.*, 2008, **602**, L89-L94.

145. L. Zhang, R. Iyyamperumal, D. F. Yancey, R. M. Crooks and G. Henkelman, *ACS Nano,* 2013, **7**, 9168−9172.

146. J. Shin, J. H. Choi, P. R. Cha, S. K. Kim, I. Kim, S. C. Lee and D. S. Jeong, *Nanoscale,* 2015, **7**, 15830−15839.

147. Y. Yang, C. Dai, Y. Shen, A. Fisher and D. Cheng, *Int. J. Hydrog. Energy*, 2016, **41**, 13014-13023.

148. P. C. Jennings, H. A. Aleksandrov, K. M. Neyman and R. L. Johnston. *J. Phys. Chem. C*, 2015, **119**, 11031−11041.

149. P. C. Jennings, H. A. Aleksandrov, K. M. Neyman and R. L. Johnston, *Nanoscale*, 2014, **6**, 1153−1165.

150. P. C. Jennings, H. A. Aleksandrov, K. M. Neyman and R. L. Johnston, *Phys. Chem. Chem. Phys.*, 2014, **16**, 26539-26545.

151. X. Huang, Z. Zhao, L. Cao, Y. Chen, E. Zhu, Z. Lin, M. Li, A. Yan, A. Zettl, Y. M. Wang, X. Duan, T. Mueller and Y. Huang, *Science*, 2015, **348**, 1230-1234.

152. A. Orfanidi P. Madkikar, H. A. El-Sayed, G. S. Harzer, T. Kratky and H. A. Gasteiger, *J. Electrochem. Soc.*, 2017, **164**, F418-F426.

153. L. Cao and T. Mueller, *J. Phys. Chem. C*, 2015, **119**, 17735−17747.

154. T. Eom, W. J. Kim, H.-K. Lim, M. H. Han, K. H. Han, E.-K. Lee, S. Lebègue, Y. J. Hwang, B.K. Min and H. Kim, *J. Phys. Chem. C*, 2018, **122,** 169245-9254.

155. Q. Jia, Z. Zhao, L. Cao, J. Li, S. Ghoshal, V. Davies, E. Stavitski, K. Attenkofer, Z. Liu, M. Li, X. Duan, S. Mukerjee, T. Mueller and Y. Huang, *Nano Lett.* 2018, **18**, 798−804.

156. V. Beermann, M. Gocyla, E. Willinger, S. Rudi, M. Heggen, R. E. Dunin-Borkowski, M.-G. Willinger and P. Strasser, *Nano Lett.*, 2016, **16**, 1719–1725.

157. L.-L. Wang and D. D. Johnson, *J. Am. Chem. Soc.*, 2009, **131**, 14023-14029.

158. A. Mahata and B. Pathak, *Nanoscale*, 2017, **9**, 9537–9547.

159. C. Chen, Y. Kang, Z. Huo, Z. Zhu, W. Huang, H. L. Xin, J. D. Snyder, D. Li, J. A. Herron, M. Mavrikakis, M. Chi, K. L. More, L. Li, M. M. Markovic, G. A. Somorjai, P. Yang and V. R. Stamenkovic, *Science*, 2014, **343**, 1339-1343.

160. C. Wang, L. Zhang, H. Yang, J. Pan, J. Liu, C. Dotse, Y. Luan, R. Gao, C. Lin, J. Zhang, J. P. Kilcrease, X. Wen, S. Zou and J. Fan, *Nano Lett.*, 2017, **17**, 2204−2210.

161. N. Becknell, Y. Kang, C. Chen, J. Resasco, K. Kornienko, J. Guo, N. M.Markovic, G. A. Somorjai, V. R. Stamenkovic and P. Yang, *J. Am. Chem. Soc.*, 2015, **137**, 15817−15824.

162. L. Zhang, L. T. Roling, X. Wang, M. Vara, M. Chi, J. Liu, S.-II. Choi, J. Park, J. A. Herron, Z. Xie, M. Mavrikakis and Y. Xia, *Science*, 2015, **349**, 412-416.

163. X. Wang, L. F. Cosme, X. Yang, M. Luo, L. Liu, Z. Xie and Y. Xia, *Nano Lett.*, 2016, **16**, 1467−1471.

164. A. Mahata, K. S. Rawat, I. Choudhuri and B. Pathak, *J. Mater. Chem. A*, 2016, **4**, 12756–12767.

165. M. J. Allen, V. C. Tung and R. B. Kaner, *Chem. Rev.*, 2010, **110**, 132-145.

166. K. S. Novoselov, E. McCann, S. V. Morozov, V. I. Fal'ko, M. I. Katsnelson, U. Zeitler, D. Jiang, F. Schedin and A. K. Geim, *Nat. Phys.*, 2006, **2**, 177−180.

167. S. Gupta, A. Kutana and B. I. Yakobson, *J. Phys. Chem. Lett.*, 2018, **9**, 2757-2762.

168. Y. Ding, X. Zhu, S. Xiao, H. Hu, L. H. Frandsen, N. A. Mortensen and K. Yvind, *Nano Lett.*, 2015, **15**, 4393-4400.

169. P. Lu, L. Wu, C. Yang, D. Liang, R. Quhe, P. Guan and S. Wang, *Scientific Reports,* 2017, **7**, 3912.

170. Z. Wang, C. Tang, R. Sachs, Y. Barlas and J. Shi, *Phys. Rev. Lett.*, 2015, **114**, 016603.

171. H. S. S. R. Matte, K. S. Subrahmanyam and C. N. R. Rao, *J. Phys. Chem. C*, 2009, **113**, 9982-9985.

172. M. Hu, Z. Yao and X. Wang, *Ind. Eng. Chem. Res.*, 2017, **56**, 3477-3502.

173. Y. Jiao, Y. Zheng, M. Jaroniec and S. Z. Qiao, *J. Am. Chem. Soc.*, 2014, **136**, 4394-4403.

174. K. Uosaki, G. Elumalai, H. Noguchi, T. Masuda, A. Lyalin, A. Nakayama and T. Taketsugu, *J. Am. Chem. Soc.*, 2014, **136**, 6542-6545.

175. P. Zhang, B. B. Xiao, L. Hou, Y. F. Zhu, and Q. Jiang, *Scientific Reports*, 2014, **4**, 3821.

176. X. Huang, S. Tang, X. Mu, Y. Dai, G. Chen. Z. Zhou, F. Ruan, Z. Yang and N. Zheng, *Nat. Nanotechnol.*, 2011, **6**, 28-32.

177. K. Jang, H. J. Kim and S. U. Son, *Chem. Mater.*, 2010. **22**, 1273–1275.

178. A.-X. Yin, W-C. Liu, J. Ke, W. Zhu, J. Gu, Y-CH. Zhang and C.-H. Yan, *J. Am. Chem. Soc.*, 2012, **134**, 20479–20489.

179. L. Bu, N. Zhang, S. Guo, X. Zhang, L. Li, L. Yao, T. Wu, G. Lu, J-U. Ma, D. Su and X. Huang, *Science*, 2016, **354**, 1410-1414.

180. C. Koenigsmann, M. E. Scofield, H. Liu and S. S. Wong, *J. Phys. Chem. Lett.*, 2012, **3**, 3385-3398.

181. Y. T. Liang, C. W. Liu, H. S. Chen, T. J. Lin, C. Y. Yang, T. L. Chen, C. H. Lin, M. C. Tu and K. W. Wang, *RSC Adv.,* 2015, **5**, 39205-39208.

182. S. M. Kim, L. Liu, D. J. Kim and S. Park, *J. Phys. Chem. C*, 2015, **119**, 23075-23081.

183. S. Fu, C. Zhu, J. Song, M. H. Engelhard, H. Xia, D. Du and Y. Lin, *ACS Appl. Mater. Interfaces*. 2016, **8**, 35213-35218.

184. W. Wang, F. Lv, B. Lei, S. Wan, M. Luo and S. Guo, *Adv. Mater*. 2016, **28**, 10117-10141.

185. K. Jiang, D. Zhao, S. Guo, X. Zhang, X. Zhu, J. Guo, G. Lu and X. Huang, *Sci. Adv.,* 2017, **3,** e1601705.

186. M. Li, Z. Zhao, T. Cheng, A. Fortunelli, C.-Y. Chen, , R. Yu, Q. Zhang, L. Gu, M. B. V. Merinov, Z. Lin, E. Zhu, T. Yu, Q. Jia, J. Guo, L. Zhang, W. A. Goddard III, Y. Huang and X. Duan, *Science*, 2016, **354**, 1414-1419.

187. T. G. Gambu, M. A. Petersen and E. V. Steen, *Catalysis Today*. 2017, **312**, 126-131.

188. I. Matanovic ́, P. R. C. Kent, F. H. Garzon and N. J. Henson. *J. Phys. Chem. C*, 2012, **116**, 16499-16510.

189. A. S. Nair, A. Mahata and B. Pathak, *ACS Appl. Energy. Mater.*, 2018, **1**, 3890-3899.

190. S. Yang, J. Kim, Y. J. Tak, A. Soon and H. Lee, *Angew. Chem. Int. Ed.*, 2016, **55**, 2058-2062.

Catalysis Science & Technology Accepted Manuscript

191. C. H. Choi, M. Kim, H. C. Kwon, S. J. Cho, S. Yun, H.-T. Kim. H.-T. Mayrhofer, H. Kim and M. Choi, *Nat. Commun.*, 2016. **7**, 10922.

192. C. Zhu, Q. Shi, S. Feng, D. Du and Y. Lin, *ACS Energy Lett.*, 2018, **3**, 1713-1721.

193. X. Li, W. Zhong, P. Cui, J. Li and J. Jiang, *J. Phys. Chem. Lett.*, 2016, **7**, 1750-1755.

194. J. Liu, M. Jiao, L. Lu, H. M. Barkholtz, L. Li, Y. Wang, L. Jiang, Z. Wu, D. Liu. L. Zhuang, C. Ma, J. Zeng, B. Zhang, B. Su, P. Song, X. Xing, W. Xu, Y. Wang, Z. Jiang and Sun, G. *Nat. Comm.*, 2017, **8**, 15938.

195. S. Back, A. R. Kulkarni and S. Siahrostami, *ChemCatChem.*, 2018, **10**, 1-7.

196. C. B. Krishnamurthy, O. Lori, L. Elbaz and I.Grinberg, *J. Phys. Chem. Lett.*, 2018, **9**, 2229-2234.

197. F. Vin˜es, J. R. B. Gomes, F. Illas, *Chem. Soc. Rev.*, 2014, **43**, 4922-4939.

198. H. R. Dakhel, P. Mirau, R. R. Naik, M. R. Knechtc and H. Heinz, *Phys. Chem. Chem. Phys.*, 2013, **15**, 5488-5492.

199. Y. Tanga and W. Cheng, *Nanoscale*, 2015, **7**, 16151-16164.

200. H.-E. Lee, K. D. Yang, S. M. Yoon, H.-M. Ahn, Y. Y. Lee, H. Chang, D. H. Jeong, Y.-S. Lee, M. Y. Kim and K. T. Nam, *ACS Nano*, 2015, **9**, 8384-8393.

201. M. H. Huang, S. Rej and S.-C. Hsu, *Chem. Commun.*, 2014, **50**, 1634-1644.

202. T. S. Ahmadi, Z. L. Wang, T. C. Green, A. Henglein and M. A. El-Sayed, *Science*, 1996, **272**, 1924-1925.

203. R. Narayanan and M. A. El-Sayed, *J. Phys. Chem. B*, 2004, **108**, 5726-5733.

204. R. Narayanan and M. A. El-Sayed, *J. Am. Chem. Soc.*, 2004, **126**, 7194-7195.

205. C. Wang, H. Daimon, T. Onodera, T. Koda and S.A. Sun, *Angew. Chem. Int. Ed.*, 2008, **47**, 3588 –3591.

206. C. Wang, H. Daimon, T. Onodera, T. Koda and S. A Sun, *Angew. Chem.*, 2008,**120**, 3644–3647.

207. C. M. S. Sa´nchez, J. Solla-Gullo´, F. J. Vidal-Iglesias, A. Aldaz, V. Montiel and E. Herrero, *J. Am. Chem. Soc.*, 2010, **132**, 5622-5624.

208. J. Zhang, H. Yang, J. Fang and S. Zou, *Nano Lett.*, 2010, **10**, 638-644.

209. J. Wu, J. Zhang, Z. Peng, Z. Yang, F. T. Wagner and H. Yang, *J. Am. Chem. Soc.*, 2010, **132**, 4984-4985.

210. J. Wu, L. Qi, H. You, A. Gross, J. Li and H. Yang, *J. Am. Chem. Soc.*, 2012, **134**, 11880-11883.

211. M. Rück, A. Bandarenk, F. Calle-Vallejo and A.Gagliardi*, Nanoscale Adv.*, 2019, Advance Article (DOI: 10.1039/C9NA00252A)

212. J. Gielis*, Am. J. Bot.*, 2003, **90**, 333–338.

213. M. K. Baek, J. B. Park and K. Y. Lee, *IFAC-Papers OnLine*, 2016, **49**, 284–289.

214. R. Reske, H. Mistry, F. Behafarid, B. R. Cuenya and P. Strasser, *J. Am. Chem. Soc.*, 2014, **136**, 6978-6986.

215. S. Cao, F. Tao, Y. Tang, Y. Lia and J. Yu, *Chem. Soc. Rev.*, 2016, **45**, 4747-4765.

216. M. Arenz, K. J. J. Mayrhofer, V. R. Stamenkovic, B. B. Blizanac, T. Tomoyuki, P. N. Ross and N. M. Markovic, *J. Am. Chem. Soc.*, 2005, **127**, 18, 6819-6829.

217. S. Chen, R. W. Murray and S. W. Feldberg,. *J. Phys. Chem. B*, 1998, **102**, 9898-9907.

218. S. Chen, R. S. Ingram, M. J. Hostetler, J. J. Pietron, R. W. Murray, T. J. Schaaff, J. T. Khoury, M. M. Alvarez and R. L. Whetten, *Science*, 1998, **280**, 2098-2101.

219. G. A. Tritsaris, J. Greeley, J. Rossmeisl and J. K. Nørskov, *Catal Lett*., 2011, **141**, 909–913.

220. J. X. Wang, H. Inada, L. Wu, Y. Zhu, Y. M. Choi, P. Liu, W.-P. Zhou and R. R. Adzic, *J. Am. Chem. Soc*., 2009, **131**, 17298-17302.

221. W. An and P. Liu, *J. Phys. Chem. C*, 2013, **117**, 16144-16149.

222. F. J. Perez-Alonso, D. N. McCarthy, A. Nierhoff, P. H. Fernandez, C. Strebel, , I. E. L. Stephens, J. H. Nielsen and I. Chorkendorff, *Angew. Chem. Int. Ed*., 2012, **51**, 4641-4643.

223. I. N. Leontye, S. V. Belenov, V. E. Guterman, P. Haghi-Ashtiani, A. P. Shaganov and B. Dkhil, *J. Phys. Chem. C*, 2011, **115,** 5429-5434.

224. M. Shao, A. Peles and K. Shoemaker, *Nano Lett.* 2011, **11**, 3714-3719.

225. M. Nesselberger, S. Ashton, J. C. Meier, I. Katsounaros, K. J. J. Mayrhofer and M. Arenz, *J. Am. Chem. Soc.,* 2011, **133**, 17428-17433.

226. B. Garlyyev, K. Kratzl, M. Rgck, J. Michalicˇka, J. Fichtner, J. M. Macak, T. Kratky, S. Ggnther, M. Cokoja, A. S. Bandarenka, A. Gagliardi and R. A. Fischer, *Angew. Chem. Int. Ed*., 2019, **58**, 9596 –9600.

227. S. Bhattacharjee and S. C. Lee, *J. Phys. Chem. C*, 2018, **122,** 894-901.

228. J. Xiao, L. Kou, C.-Y. Yam, T. Frauenheim and B. Yan, *ACS Catal*., 2015, **5,** 7063-7067.

229. P.-Y. Cai, Y.-W. Huang, Y.-C. Huang, M.-C. Cheng, L.-W. Lan, C.-C. Kuo, J.-H. Wang and M.-F. Luo. *J. Phys. Chem. C*, 2018, **122**, 16132−16141.

230. X. Xia, S. Chen, W. Ding, Y. Ni and Z. Wei, *Chem. Commun.*, 2013, **49**, 10112-

Table of Content
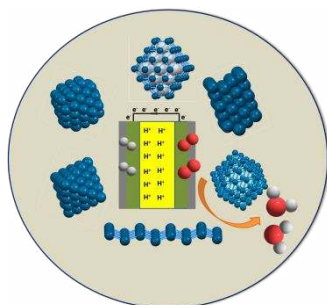
A comprehensive evaluation of Pt-nanostructure based electrocatalysts for oxygen reduction reaction